



HAL
open science

The impact of the heteroatom in a five-membered ring on the photophysical properties of difluoroborates

Anna Grabarz, Beata Jędrzejewska, Agnieszka Skotnicka, N. Arul Murugan, Filip Patalas, Wojciech Bartkowiak, Denis Jacquemin, Borys Ośmiałowski

► **To cite this version:**

Anna Grabarz, Beata Jędrzejewska, Agnieszka Skotnicka, N. Arul Murugan, Filip Patalas, et al.. The impact of the heteroatom in a five-membered ring on the photophysical properties of difluoroborates. *Dyes and Pigments*, 2019, 170, pp.107481. 10.1016/j.dyepig.2019.04.026 . hal-03450839

HAL Id: hal-03450839

<https://hal.science/hal-03450839v1>

Submitted on 20 Dec 2021

HAL is a multi-disciplinary open access archive for the deposit and dissemination of scientific research documents, whether they are published or not. The documents may come from teaching and research institutions in France or abroad, or from public or private research centers.

L'archive ouverte pluridisciplinaire **HAL**, est destinée au dépôt et à la diffusion de documents scientifiques de niveau recherche, publiés ou non, émanant des établissements d'enseignement et de recherche français ou étrangers, des laboratoires publics ou privés.



Distributed under a Creative Commons Attribution - NonCommercial 4.0 International License

1 The Impact of the Heteroatom in a Five-Membered Ring on the
2 Photophysical Properties of Difluoroborates

3 Anna Grabarz^a, Beata Jędrzejewska^b, Agnieszka Skotnicka^b, N. Arul Murugan^c, Filip
4 Patalas^d, Wojciech Bartkowiak^a, Denis Jacquemin^{e,*}, Borys Ośmiałowski^{d,*}

5 ^a*Department of Physical and Quantum Chemistry, Faculty of Chemistry, Wrocław University of
6 Technology, Wyb. Wyspiańskiego 27, PL-50370 Wrocław, Poland*

7 ^b*Faculty of Chemical Technology and Engineering, UTP University of Science and Technology,
8 Seminaryjna 3, PL-85326 Bydgoszcz, Poland*

9 ^c*Division of Theoretical Chemistry and Biology, School of Biotechnology, Royal Institute of
10 Technology, SE-10691 Stockholm, Sweden*

11 ^d*Faculty of Chemistry, Nicolaus Copernicus University, Gagarina 7, PL-87100 Toruń, Poland*

12 ^e*Laboratoire CEISAM, UMR CNRS 6230, Université de Nantes, 2 Rue de la Houssinière, BP92208,
13 44322 Cedex 3 Nantes, France*

14 **Abstract**

15 A series of novel BF₂ complexes, bearing a five-membered heterocyclic ring (with X=NMe,
16 O, and S), were synthesized and characterized with a focus on the influence of atom ex-
17 change on the photophysical properties of both unsubstituted and dimethylamino deriva-
18 tives. The experimental results show that the optical spectra substantially differ in both
19 sets of dyes. In particular, the dimethylamino series are more strongly affected by het-
20 eroatom substitution, i.e., the insertion of X=O or X=S in lieu of X=NMe causes sub-
21 stantial bathochromic shifts of the absorption and emission bands, as well as marked
22 changes in their topologies. In contrast, the optical spectra of the unsubstituted com-
23 pounds undergo only relatively small redshifts, and no variation of band shapes is ob-
24 served. Moreover, the measured absorption spectra of the unsubstituted compounds
25 bearing X=NMe and X=O are almost identical. Interestingly, the fluorescence yields
26 of the dimethylamino derivatives are much larger (up to one order of magnitude) than
27 those of the corresponding unsubstituted compounds. The experimental analyses are
28 supported by state-of-the-art quantum chemistry calculations, which satisfactorily re-
29 produced the experimental trends and provided further insights into the observed optical
30 signatures.

31 *Keywords:* TD-DFT, difluoroborates, functionalization, charge transfer

*Corresponding author

Email addresses: Denis.Jacquemin@univ-nantes.fr (Denis Jacquemin),
borys.osmialowski@umk.pl (Borys Ośmiałowski)

Preprint submitted to Dyes & Pigments

April 10, 2019

32 1. Introduction

33 Structure-optical property relationships are now established for many classes of dyes,
34 and one can often safely predict the evolution of absorption spectra with chemical sub-
35 stitution. This is more difficult to achieve for emission, which is a key challenge in view
36 of its use in many biomedical imaging applications. Indeed, there is a need to design new
37 fluorescent probes, effectively exhibiting sensitivity to environmental changes, physiolog-
38 ical conditions and/or to specific interactions ongoing in biomacromolecules. To achieve
39 these goals, countless syntheses have been carried out to functionalize fluorophores and
40 tune their emissive properties, which can be achieved through standard variation of
41 the substituent(s) [1–6], benzannulation [7–12], elongation of the π -conjugated spacer
42 separating the donor and acceptor moieties in push-pull systems [13–17], or introduc-
43 tion of additional chromophores into their structure [18–20]. However, the addition of
44 several substituents may lead to undesired effects such as the decrease of the fluores-
45 cence quantum yield (Φ_{fl}) inherent to flexible side group that enhance the efficiency of
46 non-radiative pathways. This explains why the most potent fluorescent molecules re-
47 main “simple and rigid” derivatives, e.g., xanthenes [21–25], cyanines [26–30], BODIPYs
48 [26; 31–35], and coumarins [36–40]. Among these classes, BODIPY derivatives occupy
49 a privileged position [41], because they can be easily functionalized and are very pho-
50 tostable, explaining the undisputed popularity in this family [42–46]. However, one of
51 the main disadvantages of regular BODIPY fluorophores is the impossibility to directly
52 doubly-benzannulate their five-membered rings. Indeed, while single benzannulation has
53 been achieved [47–49] and has shown to be an efficient strategy for red-shifting their
54 absorption and fluorescence maxima, double benzannulation has only been achieved at
55 other positions [50–53]. It is also well recognized that atom exchange, leading to iso-
56 electronic compounds, may significantly impact the photophysical signatures of dyes. In
57 fluoroborate dyes, substituent, benzannulation, and π -extension have been extensively
58 applied to tune the photophysical properties, but atom exchange has been relatively less
59 studied, though fluorescent techniques are also well suited to assess the impact of the

60 changes induced by atom-by-atom substitutions. In the classes of dyes encompassing
 61 atom-substituted BODIPYs, one should, of course mention: i) aza-BODIPY dyes – with
 62 a nitrogen atom at the *meso* position – that shows red-shifted optical bands compared to
 63 standard BODIPYs [54–58]; ii) other difluoroborates showing one or both nitrogen atoms
 64 in their N-BF₂-N core replaced by oxygen atoms, e.g., boranils [59–62], hydroxyphenyl-
 65 benzoxazole (HBO) complexes [63–65], difluoroboron β -diketonate complexes [66–68],
 66 and others [42; 69–71] (see Figure 1).

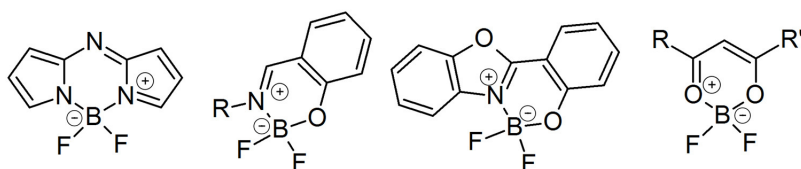
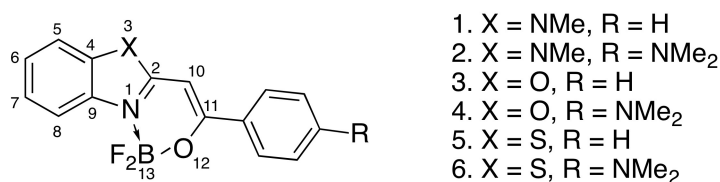


Figure 1: The common derivatives of BODIPY dyes, from left to right: aza-BODIPY, boranils, HBO complexes and difluoroboron β -diketonate complexes.

67 Notably, in contrast to standard BODIPY compounds, some of these derivatives, e.g.,
 68 HBO complexes and boranils, are characterized by improved Stokes shifts (Δ_{ss}), usually
 69 larger than 50 nm [72–74], whereas the Δ_{ss} typically do not exceed 20 nm in standard
 70 BODIPYs [31; 41; 75]. Additionally the emission range of those compounds can be
 71 further red-shifted by extending the π -conjugated structure [76; 77]. This suggests that
 72 additional efforts to synthesize and understand the impact of atom substitution in this
 73 class of dyes are of interest. In a recent work, we have studied the impact of atom
 74 exchange directly bonded to the boron atom (OBF₂N *versus* SBF₂N) [78]. While this
 75 provided the first example of fluorophores of the BF₂ family with a S-B bond, these
 76 molecules were composed of six-membered rings only. In this context, our goal here is to
 77 synthesize NMe₂-bearing fluoroborate derivatives containing one five-membered ring and
 78 to compare their photophysical properties with their unsubstituted analogues (Scheme 1).
 79 One can expect that the impact of atom-exchange is stronger in five-membered ring
 80 than in their six-membered counterparts, because of the higher strain in the former
 81 compounds. We underline that atom exchange does not influence only the electronic

82 properties but also impacts the vibrations in the five-membered ring and, in turn, can
 83 modify the vibronic couplings and hence the absorption and fluorescence band shapes [79;
 84 80]. In more detail, we have three goals here: i) studying the effect of atom exchange on
 85 fluorophores incorporating or not a strong donor group; ii) probing the electron accepting
 86 properties of three different five-membered heterocycles; and iii) gaining insights into the
 87 electronic structure of the newly synthesized compounds using first principles calculations



Scheme 1: The general structure of BF₂-complexes of various heterocycles studied herein.

88 2. Experimental and theoretical methods

89 2.1. Experimental methods

90 The 2-phenacylheterocycles [49; 81] were first obtained and next converted to their
 91 BF₂ complexes following the procedure established for similar derivatives [50; 82]. For
 92 all presented structures NMR data (¹H, ¹¹B, ¹³C, ¹⁵N and ¹⁹F) have been obtained (see
 93 Experimental Section at the end of this work). The fluorescence yields were determined
 94 in chloroform as follows. The fluorescence spectrum of dilute (A ≈ 0.1) solutions of
 95 the compounds were recorded by excitation at the absorption band maximum of the
 96 reference (see Table S3 in the SI). The quantum yield of the tested compounds (Φ_{dye})
 97 was calculated using the following equation [83]:

$$\Phi_{\text{dye}} = \Phi_{\text{ref}} \frac{I_{\text{dye}} A_{\text{ref}}}{I_{\text{ref}} A_{\text{dye}}} \cdot \frac{n_{\text{dye}}^2}{n_{\text{ref}}^2}$$

98 where Φ_{ref} is the fluorescence yield of the reference, A_{dye} and A_{ref} are the absorbance
 99 of the dye and reference samples at the excitation wavelengths, I_{dye} and I_{ref} are the
 100 integrated emission intensity for the dyes and references samples, n_{dye} and n_{ref} are the

101 refractive indices of the solvents used for the dyes and reference, respectively. Knowing
102 the (average) lifetime of the S_1 excited state (τ_{av}) and the fluorescence quantum yield
103 (Φ_{fl}), the radiative (k_r) and nonradiative (k_{nr}) rate constants were calculated using:

$$k_r = \frac{\Phi_{fl}}{\tau_{av}}$$
$$k_{nr} = \frac{1 - \Phi_{fl}}{\tau_{av}}$$

104 2.2. Computational details

105 The geometries of the six studied compounds were optimized in their electronic ground
106 state (GS) at the B3LYP/6-311++G(d,p) level of theory. The effects of the solvent
107 ($CHCl_3$ solution is used consistently with experiment, except when noted) were included
108 by means of the linear-response variant of polarizable continuum model (LR-PCM) [84].
109 The minimal nature of the optimal GS geometries was confirmed by evaluation of the
110 Hessian. These minimum-energy geometries were used in all subsequent molecular dy-
111 namics simulations described below. In order to determine the vertical electronic spectra
112 we have applied the state-of-the-art polarizable-embedded resolution-of-identity second-
113 order coupled-cluster (PERI-CC2) method [85]. In more detail, we firstly carried out
114 molecular dynamics (MD) calculations for BF_2 -complexes in chloroform solvent and the
115 trajectories were subjected to subsequent PERI-CC2/MM calculations. During the MD
116 simulations, the interactions between the solute and solvent subsystems were described
117 considering both electrostatic and van der Waals interactions, and this requires charges
118 and force field parameters for each of the molecules. The electrostatic potential fitted
119 charges for the difluoroborates were obtained using the B3LYP/6-311++G(d,p) level of
120 theory and CHEPLG procedure [86] as implemented in Gaussian 09 software. To de-
121 scribe the van der Waals interactions, we employed General AMBER Force Field (GAFF)
122 [87] and `CHCL3.frcmod` for BF_2 -carrying and chloroform solvent molecules, respectively.
123 Selected chloroform force field includes both bond length and bond angle parameters
124 making the solvent flexible. Even though GAFF provides a flexible molecular model

125 for solutes, we treated the difluoroborates molecules with rigid body approximation.
126 The simulations for BF₂-carrying compounds in chloroform encompassed a single solute
127 molecule and a few thousands of solvent molecules. The calculations were carried out
128 at room temperature and 1 atmospheric pressure using the Amber16 software [88]. The
129 calculations were performed in an isothermal-isobaric ensemble, so that the density of
130 the solute-solvent system evolves to the right value independent of the initial density.
131 The maintenance of the system at a specific temperature and pressure has been achieved
132 by connecting the system to Langevin’s thermostat and Barendsen’s barostat. The time
133 step for integration of equation of motion was set to 2 fs and the total time scale for the
134 production run was 10 ns. The convergence of key properties (energies and density) in
135 each simulation was checked. Fifty configurations from the last 5 ns simulations selected
136 at equal intervals have been used for computing the spectra using PERI-CC2 method
137 which describes the interaction between the solute-solvent subsystems using electrostatic
138 embedding. The same force-fields as in the MD simulations were used to describe the
139 solvents during the PERI-CC2 calculations. The PERI-CC2 calculations were carried
140 out by using the Turbomole package [89].

141 Since excited-state (ES) properties, e.g., electronic density changes upon electronic
142 excitation, are not available yet at the PERI-CC2 level, we have employed the Kohn-Sham
143 formulation of time-dependent density functional theory (TD-DFT) for their determina-
144 tion. The DFT and TD-DFT calculations were performed with the Gaussian 09 package
145 [90], employing 11 different exchange-correlation functionals (XCF), i.e., BLYP [91; 92],
146 B3LYP [93], PBE0 [94; 95], M06 [96], BHandHLYP [97], CAM-B3LYP [98], M06-2X
147 [96], ω B97X [99], ω B97X-D [100], LC-BLYP [101], and M06-HF [102; 103]. Five excited
148 states were considered. For all DFT/TD-DFT calculations, we used so-called *ultrafine*
149 integration grid. The density difference plots were simulated with a 0.002 au contour
150 threshold, with density increase (decrease) indicated by red (blue) zones. Subsequent
151 charge-transfer parameters, namely the distance on which charge is transferred (d_{CT}), the
152 amount of charge (q_{CT}) and the dipole moment change upon transition ($\mu_{CT} = \mu_{ES} - \mu_{GS}$)

153 were calculated using Le Bahers’ procedure described in details elsewhere [104; 105]. In
 154 this procedure, the CT parameters are determined using the barycenters of density in-
 155 crease and decrease upon photon absorption. All calculations of transition energies were
 156 performed with the aug-cc-pVDZ basis set [106–108].

157 3. Results and discussion

158 The measured absorption and emission spectra of all six compounds obtained in
 159 chloroform are given in Figure 2 and the associated data are listed in Tables 1 and 2. Let
 160 us first discuss the results obtained for the absorption spectra. Obviously, the absorption
 161 bands of the unsubstituted compounds (R=H) are blue-shifted compared to the R=NMe₂
 162 dyes, a statement holding irrespective of the X heteroatom. Indeed, for all unsubstituted
 163 compounds (X=NMe, O, and S) the absorption band peaks at 350–375 nm, whereas for
 164 R=NMe₂ the span is twice as large (400–450 nm). In addition, both the shapes and the
 165 positions of the absorption bands of the unsubstituted X=NMe and X=O compounds
 166 are highly similar, whereas the corresponding NMe₂-substituted derivatives show more
 167 pronounced discrepancies in their band topologies. Introducing the donor group also
 168 yields a significant evolution of the band shape for the thio derivative.

Table 1: Photophysical properties of examined compounds measured in chloroform.

Struct.		λ_{abs}	λ_{fl}	ε	Δ_{ss}	Φ_{fl}^a	Φ_{fl}^b
X	R	[nm]	[nm]	[M ⁻¹ cm ⁻¹]	[cm ⁻¹]	[%]	[%]
NMe	H	349	420	21400	4844	< 1	< 1
O	H	351	424	27000	4905	< 1	< 1
S	H	369	444	26300	4578	1	< 1
NMe	NMe ₂	398	443	28000	2552	49	46
O	NMe ₂	411	457	42500	2449	98	86
S	NMe ₂	447	480	59800	1538	70	68

^a - quantum yield measured with the use of the references, ^b - quantum yield measured with the use of integrating sphere.

169 As can be seen in Table 1, the measurements of the fluorescence quantum yields for

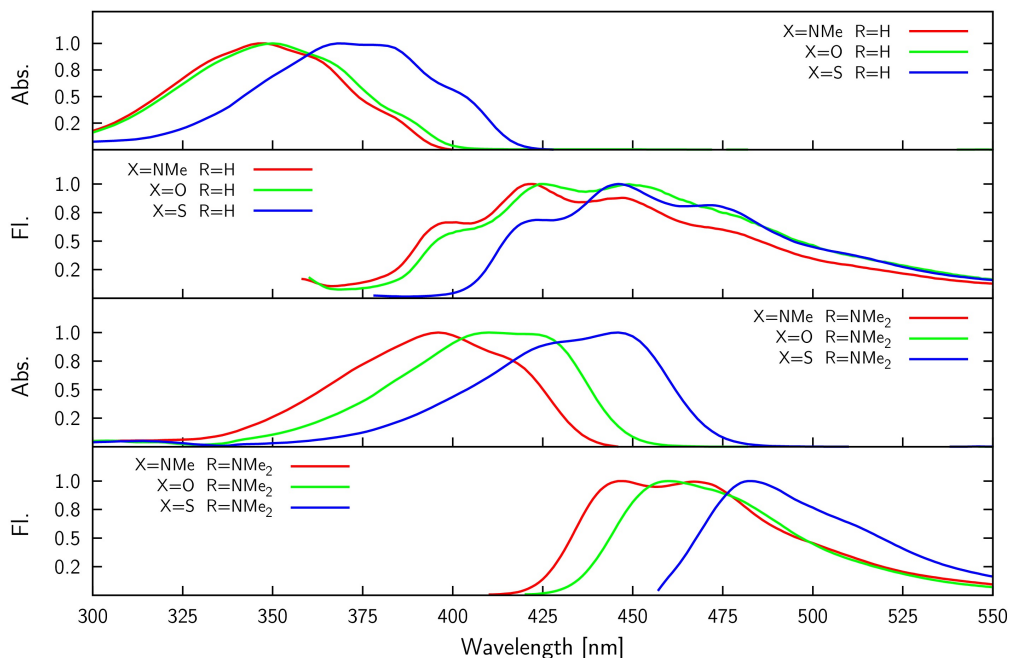


Figure 2: Experimental absorption and emission spectra in CHCl_3 .

170 R= NMe_2 dyes returned very high values (Φ_{fl} of 48.7, 98.2, and 70.0% for X= NMe , X= O
 171 and X= S respectively) thereby representing huge increases compared to their unsubsti-
 172 tuted counterparts (all $<1\%$). Clearly, the enhancement of Φ_{fl} values is also dependent
 173 on heteratom type, since in both the R= NMe_2 and R= H series, Φ_{fl} are improved fol-
 174 lowing $\text{NMe} \rightarrow \text{O}$ and/or $\text{NMe} \rightarrow \text{S}$ substitution. At this stage, we hypothesize that the
 175 vibrations and rotations around the single bonds separating the BF_2 scaffold and the
 176 side phenyl ring (see Scheme 1) that are likely to quench the emission of the dyes in
 177 solution, are significantly limited when an amino group is added. Consistently with the
 178 measured quantum yields, enhanced fluorescence lifetimes are observed for the NMe_2
 179 substituted dyes (see Table 2 and the fluorescence decay profiles in Figures S10–S15
 180 in the SI). For the unsubstituted compounds, two exponential fluorescence decays were
 181 observed (See Table 2) with a major component close to 70–90 ps and another at ca.
 182 0.9–1.8 ns. In contrast, in the NMe_2 series, the fluorescence decay profiles fit well with

183 a single-exponential function, giving fluorescence lifetimes of 0.86, 1.59 and 1.78 ns for
184 X=NMe, O, and S, respectively. In other words, in the amino series, the fluorescence
185 lifetimes increase along with the NMe→O→S pattern. From the Table 2 one also notices
186 that the radiative rate constant (k_r) increases when the compounds are substituted by
187 electron releasing substituent NMe₂, i.e., the enhancement of Φ_{fl} originates in both the
188 expected decrease of k_{nr} (*vide supra*) and the increase of k_r . The differences in the k_r
189 values for R=H series are not significant but the k_r/k_{nr} ratio between is two- or three
190 orders lower than unity, indicating that the non-radiative deactivation of S₁ is efficient.
191 The situation is opposite in the R=NMe₂: the k_r/k_{nr} ratio is close to unity for X=NMe
192 derivative and becomes even higher in the X=S and X=O derivatives.

193 Our next step was to check how solvatochromic effects affect the properties of R=H
194 and R=NMe₂ derivatives, thus we measured absorption and emission properties of the
195 examined dyes in three solvents characterized by different dielectric constant. The elec-
196 tronic absorption and fluorescence spectra recorded in methylcyclohexane (MCH), N,N-
197 dimethylformamide (DMF) and tetrahydrofuran (THF) can be found in Figures S8-S9
198 in the SI whereas the corresponding spectroscopic and photophysical properties are col-
199 lected in Tables S5 and S6. As can be seen in Figure S8, the UV-vis absorption spectra of
200 the unsubstituted difluoroborates (R=H) do not display any significant variation of their
201 absorption maxima position, when changing the solvent dielectric constant. In contrast,
202 the absorption maxima of the dimethylamine-substituted derivatives undergo positive
203 solvatochromism, e.g., a noticeable red-shift from 439 nm in MCH to 450 nm in DMF
204 is found for the X=S R=NMe₂ compound (see Figure S9 in the SI). These red-shifts of
205 the absorption maxima position along with the high molar absorption coefficients indi-
206 cate that the transitions of the R=NMe₂ derivatives have a $\pi - \pi^*$ nature associated
207 with a significant charge transfer (CT) (see Table S5). Similarly, a considerable redshift
208 driven by a solvent dielectric constant change is also observed in the emission spec-
209 tra of X=O R=NMe₂ and X=S R=NMe₂ compounds, whereas no significant shift was
210 found in the fluorescence spectra of unsubstituted difluoroborates, indicating that the

211 CT character of the first singlet excited state is much more marked in the dimethylamine
212 derivatives [109; 110]. Interestingly, the emission spectra of the X=NMe R=NMe₂ dye
213 display significantly smaller solvatochromic shifts, than their benzoxazole and benzoth-
214 iazole analogues. In short, the redshifts of the emission maxima positions, as well as
215 higher sensitivity of fluorescence spectra (with respect to absorption) to the dielectric
216 constant of the environment are characteristics of push-pull compounds undergoing CT
217 transitions [109–112].

218 As can be seen in Table S5, the fluorescence quantum yields of the unsubstituted
219 dyes remain very small (<1%), irrespective of the solvent dielectric constant. Obviously,
220 such trifling values do not allow for an unambiguous interpretation of the impact of the
221 solvent dielectric constant on the Φ_f ; the trends being however similar as in CHCl₃. In
222 contrast, the R=NMe₂ dyes fluoresce intensively in all studied solvents. The Φ_f of the
223 X=S R=NMe₂ compound is systematically decreasing with increasing solvent dielectric
224 constant, which is a usual trend in dyes exhibiting large charge separation in their excited
225 state [113; 114]. Interestingly, the opposite is observed for X=NMe R=NMe₂ dye, in
226 which fluorescence quantum yield increases from 14.5% (MCH) up to 56.5% (DMF). It
227 is not easy to interpret this peculiar behavior but we hypothesize that it is related to
228 the motion of the additional methyl group that would be somehow diminished in DMF.
229 Indeed, such improvement of the fluorescence quantum yield with increasing in solvent
230 dielectric constant, also known as negative solvatokinetic effect, might be connected
231 with interactions between the excited solute and solvent molecules, which changes the
232 excited-state configuration and the fluorescence intensity [115–120]. However, the above
233 hypothesis needs more precise studies in a wider range of solvents and is out of the scope
234 of the current work. Eventually, for X=O R=NMe₂, the Φ_f is similar in THF (68.9%)
235 than in MCH (73.5%), but a lower efficiency is observed in the most polar DMF (52.5%)
236 , as usual. We also highlight that, irrespective of the selected solvent, the unsubstituted
237 compounds exhibit a two-exponential decay emission whereas the R=NMe₂ dyes show
238 mono-exponential decays, but for X=NMe R=NMe₂ in MCH.

Table 2: Fluorescence lifetimes (τ), component amplitudes (α), correlation coefficients (χ^2) and radiative (k_r) and non-radiative (k_{nr}) rate constants for examined compounds in chloroform.

Struct.		τ_1	τ_2	α_1	α_2	τ_{av}	χ^2	k_r	k_{nr}	k_r/k_{nr}
X	R	[ps]	[ps]			[ps]		$[\text{s}^{-1}] \times 10^8$	$[\text{s}^{-1}] \times 10^8$	
NMe	H	72	1630	99.345	0.654	82.2	1.668	0.29	121	0.0024
O	H	71	1981	98.785	1.215	94.2	1.439	0.33	106	0.0031
S	H	86	1021	99.438	0.562	91.3	1.538	1.32	108	0.0120
NMe	NMe ₂	-	861	-	100	861	1.395	5.66	5.96	0.95
O	NMe ₂	-	1593	-	100	1593	1.077	6.16	0.12	53.6
S	NMe ₂	-	1775	-	100	1775	1.172	3.94	1.69	2.33

239 The fluorescence excitation and emission characteristics of all compounds have been
 240 measured in THF at different emission and excitation wavelengths. As can be seen in
 241 Figures S4 and S5 in the SI, the position of the fluorescence peaks remains constant
 242 independently of both the λ_{exc} and concentration in the solution for all compounds.
 243 This clearly suggests at a rapid internal conversion from higher excited states to the
 244 lowest vibrational energy level of the S_1 state as well as the presence of only one emitting
 245 species. In addition, the fluorescence excitation spectra were recorded for two emission
 246 wavelengths (detection at blue and red edges of the emission spectrum), as well as at
 247 the maximum of the emission spectrum for diluted and more concentrated solutions.
 248 Figures S6 and S7 display the steady-state fluorescence excitation spectra of the tested
 249 compounds, and one can observe, on the one hand, spectra independent of the considered
 250 wavelength, and, on the other hand, a non-negligible impact of the concentration of the
 251 solution. The differences between absorption and excitation spectra of the dyes in 10^{-5} M
 252 solutions show the existence of the excited molecules that differ in spatial conformations
 253 and/or solvent relaxations.

254 All these experimental results encouraged us to carry out computer simulations in
 255 order to shed light onto the electronic structure of these derivatives, one of our goals be-
 256 ing to unravel the origin of the band shape differences: multiple electronic state and/or
 257 various vibronic couplings. Our results are presented in Table 3. As can be seen, the

258 first electronic excited state is well separated from the second one, with an energy gap
259 between them attaining ca. 1 eV for all studied molecules. In addition, the oscillator
260 strengths, f are much larger for the $S_0 \rightarrow S_1$ transition (from 1.07 to 1.59) than for the
261 $S_0 \rightarrow S_2$ transition (from 0.02 to 0.06). This clearly indicates that the observed spectra
262 are solely due to the first electronic ES. For that excitation, the NMe₂-substituted com-
263 pounds exhibit larger oscillator strengths than their unsubstituted counterparts. We note
264 that the predicted f values are rather consistent with measured molar absorptivities (see
265 ϵ in Table 1): in both cases, significantly lower values are obtained for R=H derivatives.
266 Nevertheless, based on the measurements, one would have expected significantly lower
267 oscillator strength for the X=NMe R=NMe₂ derivative. Figure 3 shows the simulated
268 vertical absorption spectra in the 300–550 nm range, considering the absorption bands of
269 the $S_0 \rightarrow S_1$ transition. As discussed above, the PERI-CC2 calculations were performed
270 based on 50 solute-solvent configurations (for each compound) considering rigid dyes and
271 flexible chloroform molecules. Therefore, the widths of the absorption bands shown in
272 Figure 3 originate from the inhomogeneous broadening due to solute-solvent interactions,
273 whereas the vibronic couplings are neglected, so that the band widths are logically under-
274 estimated compared to experiment. Nevertheless, by comparing the R=H and R=NMe₂
275 derivatives, one clearly notices that the latter are much more sensitive to the solvent
276 microenvironment, explaining the larger inhomogeneous broadening of derivatives pos-
277 sessed a dimethylamino group (see the σ values in Table 3), a feature that can be directly
278 associated with an increase of the intramolecular charge-transfer character when adding
279 the electron-donating group. As neither the presence of multiple electronic states nor
280 explicit solvent-solute interactions can explain the presence of several maxima/shoulders
281 in the absorption spectra of Figure 2, these band shapes should reflect the changes in the
282 vibrational fine structure induced by chemical modifications. To confirm this hypothesis,
283 complementary calculations were performed using CC2 method, but in gas phase (see
284 Figure S3 in the SI). Although these calculations do not account for the solvent envi-
285 ronment, and hence, logically yield band positions that are blue-shifted compared to the

286 measurements and PERI-CC2 results, one notices that the experimental band shapes are
 287 reasonably well reproduced, confirming the vibronic nature of the multi-peak absorption
 288 bands.

Table 3: Average vertical excitation energies ($\overline{\Delta E}$), standard deviations of ΔE distributions ($\sigma(\Delta E)^*$) and average oscillator strengths (\bar{f}) computed at the PERI-CC2/aug-cc-pVDZ level of theory in chloroform. *FWHM= $2\sqrt{2\ln\sigma(\Delta E)}$.

Struct.		$\overline{\Delta E}$ [eV]	$\overline{\Delta E}$ [nm]	$\sigma(\Delta E)$ [eV]	\bar{f}
X	R	$S_0 \rightarrow S_1$			
NMe	H	3.73	333	0.01	1.12
O	H	3.70	335	0.01	1.12
S	H	3.44	361	0.01	1.07
NMe	NMe ₂	3.19	389	0.05	1.59
O	NMe ₂	3.07	404	0.05	1.59
S	NMe ₂	2.90	428	0.06	1.57
		$S_0 \rightarrow S_2$			
NMe	H	4.73	262	0.02	0.02
O	H	4.66	266	0.04	0.02
S	H	4.42	280	0.05	0.05
NMe	NMe ₂	4.19	296	0.03	0.06
O	NMe ₂	4.20	295	0.02	0.06
S	NMe ₂	4.00	310	0.02	0.03

289 Let us now assess the accuracy of the PERI-CC2 method in reproducing the aux-
 290 ochromic shifts on the absorption spectra. In Table 4 the experimental and simulated
 291 spectral shifts of the $S_0 \rightarrow S_1$ absorption band maxima are listed. In that Table, we
 292 used the X=NMe R=H compound as a reference. The experimentally determined shift
 293 upon X=NMe \rightarrow O replacement is trifling for R=H (+2 nm) but significant for R=NMe₂
 294 (+14 nm). The respective shifts predicted by the PERI-CC2 method are +3 nm and
 295 +15 nm, thus demonstrating the excellent agreement with experimental data. Signifi-
 296 cantly larger auxochromic effects are observed experimentally for the X=NMe \rightarrow S sub-
 297 stitution, i.e., +20 nm for R=H and +50 nm for R=NMe₂, with again simulated shifts
 298 in good agreement (+28 nm and +40 nm). One can therefore conclude that the overall

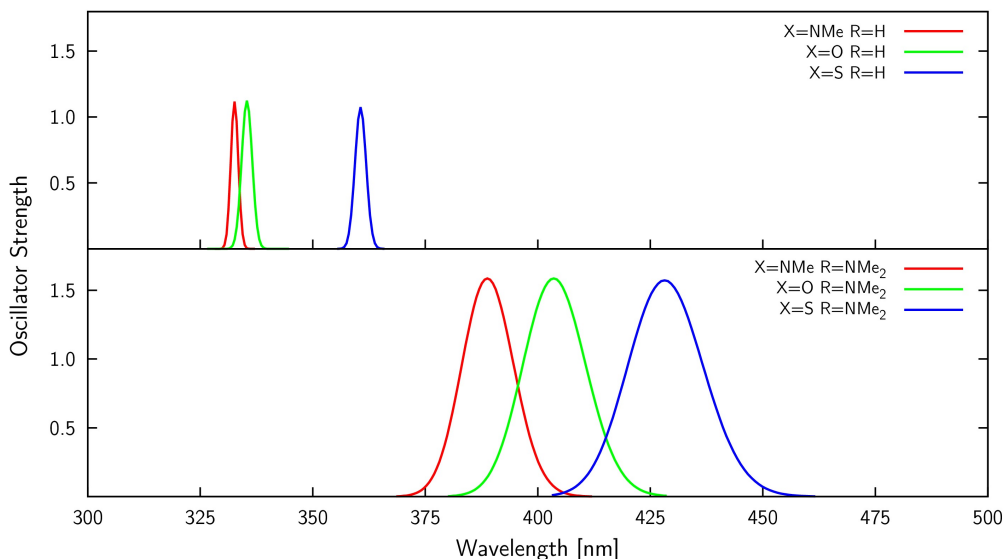


Figure 3: Electronic vertical absorption spectra simulated at the PERI-CC2/aug-cc-pVDZ level of theory.

299 agreement between the PERI-CC2 simulation results and the experimental data is, at
 300 the very least, satisfactory, thus further consolidating the above conclusions regarding
 301 the origin of the specific band shapes.

302 In order to obtain additional insights into the electronic structure of the dyes, we have
 303 probed the nature of the excited state properties in the Franck-Condon region. Since
 304 ES properties cannot yet be determined with the PERI-CC2 approach, we have turned
 305 towards TD-DFT. The performance of TD-DFT in predicting ES properties is known to
 306 significantly depend on the selected XCF [121; 122], and no single XCF can be consid-
 307 ered as outperforming the others on a systematic basis. Hence, in order to select a XCF
 308 providing accurate results for the molecules under investigation, we have benchmarked
 309 eleven XCFs and compared the obtained GS and ES dipole moments to CC2 reference
 310 values. The dipoles were chosen as they are a measure of the quality of the electronic
 311 density and are also directly related to the CT character of the electronic transition.
 312 These benchmark calculations were performed for isolated (no solvent) molecules. As
 313 can be seen in Figure 4, the errors made by DFT for GS dipole moments (μ_{GS}) are sub-

Table 4: Excitation energy changes, w.r.t. X=NMe R=H compound, induced by chemical modifications: comparisons between theory (PERI-CC2 and PCM-TD-B3LYP) and experiment.

Struct.		$S_0 \rightarrow S_1$					
X	R	exp.	exp.	PERI-CC2	PERI-CC2	PCM-TD-B3LYP	PCM-TD-B3LYP
		[eV]	[nm]	[eV]	[nm]	[eV]	[nm]
NMe	H	0.00	0	0.00	0	0.00	0
O	H	-0.02	+2	-0.03	+3	0.00	0
S	H	-0.19	+20	-0.29	+28	-0.17	+18
NMe	NMe ₂	-0.43	+48	-0.54	+56	-0.37	+43
O	NMe ₂	-0.54	+62	-0.66	+71	-0.42	+50
S	NMe ₂	-0.78	+98	-0.83	+96	-0.57	+70

314 stantially smaller compared to the TD-DFT errors for the ES (μ_{ES}), which is consistent
 315 with previous benchmarks [123; 124]. As a consequence, the errors in the so-called excess
 316 dipole moments ($\mu_{GS}-\mu_{ES}$) are mainly originating from the TD-DFT part. For the μ_{GS}
 317 the smallest errors are reached with the ω B97X XCF (smaller than 0.2 D), although
 318 all XCFs provide satisfying results. In contrast, for the ES, ω B97X yields the largest
 319 maximum deviations (ca. 3.0 D), whereas B3LYP provides the smallest maximum error
 320 for both μ_{ES} (1.3 D) and $\mu_{ES}-\mu_{GS}$ (1.9 D). B3LYP also gives one of the smallest average
 321 errors for μ_{GS} (0.3 D), μ_{ES} (1.2 D), and $\mu_{ES}-\mu_{GS}$ (1.3 D). In addition, this XCF accu-
 322 rately reproduces the impact of chemical substitution on the ES dipoles, but for a slight
 323 underestimation of the dipole increase when adding the dimethylamino group. Therefore
 324 we select B3LYP for our analysis of the ES properties in CHCl_3 solution. As can be seen
 325 in Table 4, PCM-TD-B3LYP also fairly reproduces all auxochromic shifts though less
 326 accurately than with PERI-CC2, as expected. We are well aware of the inherent limits
 327 of B3LYP for describing long-range CT systems [122], but the molecules considered are
 328 probably compact enough so that these limits are not relevant here.

329 Table 5 provides a summary of the TD-DFT ES properties computed in the Franck-
 330 Condon region together with electron density difference (EDD) plots showing the elec-
 331 tronic reorganization accompanying the transition to the lowest electronic excited state.

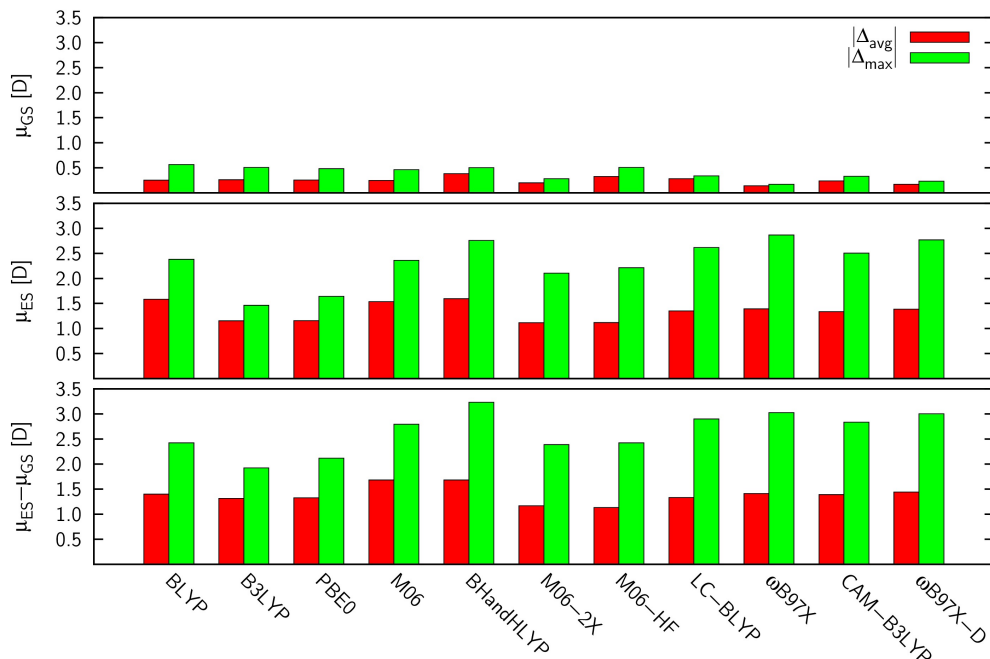


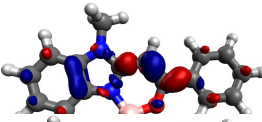
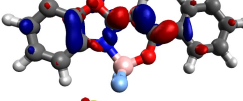
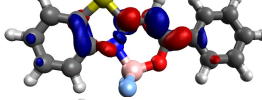
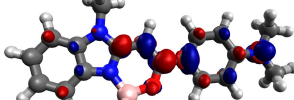
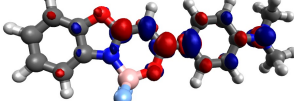
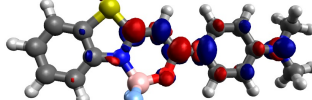
Figure 4: Errors in TD-DFT dipole moments: maximum (Δ_{max}) and average (Δ_{avg}) absolute errors compared to CC2 (see also corresponding Table S1 in the SI). All results were obtained in gas phase with the *aug-cc-pVDZ* basis set.

332 As can be seen, for the R=H compounds, the electronic density changes mainly take
 333 place within the BF_2 -containing core and adjacent five-membered ring. In contrast for
 334 molecules bearing a NMe_2 group, the density changes involve not only the BF_2 -carrying
 335 ring but also the side NMe_2 -phenyl moiety, the amino group acting, as expected, as a
 336 donor (mostly in blue in the EDDs). The CT character of the transitions in NMe_2 deriva-
 337 tives is reflected by the significant values of the dipole moment differences ($\mu_{\text{ES}} - \mu_{\text{GS}}$)
 338 which exceed 6 D for all three dyes, whereas significantly smaller values are obtained for
 339 the R=H derivatives. Logically, the charge-transfer distances d_{CT} are increasing upon
 340 NMe_2 substitution (up to $d_{\text{CT}} \approx 2.7 \text{ \AA}$). However as one can see the d_{CT} values of
 341 X=NMe R=H ($d_{\text{CT}} = 2.310 \text{ \AA}$) and X=O R=H ($d_{\text{CT}} = 2.110 \text{ \AA}$) derivatives are much
 342 closer to their NMe_2 -substituted counterparts, than to X=S R=H ($d_{\text{CT}} = 1.539 \text{ \AA}$). This
 343 can be explained by looking at the EED of R=H derivatives collected in Table 5, as one

344 can see both X=O and X=NMe derivatives have red (accepting) lobes on the bond con-
345 necting the fluoroborate core to the adjacent phenyl ring. This indicates that d_{CT} in fact
346 should be larger for those two derivatives. Additionally, the R=NMe₂ compounds are
347 also characterized by a larger transferred charge (q_{CT} of ca. 0.50 e) than in their R=H
348 counterparts (q_{CT} in the 0.41–0.43 e range). In the R=H series the CT character of the
349 electronic transition is clearly decreasing following X=NMe→O→S, which is confirmed
350 by a systematic decrease of both the d_{CT} (NMe→O=0.209 Å, O→S=0.562 Å) and μ_{ES} -
351 μ_{GS} (NMe→O=-0.395 D, O→S=-1.332 D) parameters. An interesting observation can
352 be made by comparing NMe₂-substituted compounds, i.e., d_{CT} and μ_{ES} - μ_{GS} values are
353 lowest for X=O (d_{CT} =2.713 Å, μ_{ES} - μ_{GS} =6.537 D), while opposite to R=H, the highest
354 values are obtained for the thio derivatives (d_{CT} =2.751 Å, μ_{ES} - μ_{GS} =6.612 D). In turn
355 X=NMe d_{CT} values are close to X=O, whereas μ_{ES} - μ_{GS} results are similar to those of
356 X=S. Comparing the parameters of Table 5 to the fluorescence quantum yields, one no-
357 tices that the decrease of the d_{CT} and μ_{ES} - μ_{GS} promotes the radiative transition for all
358 three dyes of each series (R=H and R=NMe₂), e.g., in the R=H series the quantum yield
359 decreases with increasing CT character. In contrast, Φ_f is much higher in the NMe₂
360 series, although the CT character is enhanced in the latter. We hypothesize that this
361 result comes from the fact that in the amino dyes, the CT involves the electron lone pair
362 of the amino nitrogen, which allows the formation of a quinoidal structure, and hence
363 lead to the rigidification of the excited state. That conclusion is also supported by the
364 single-exponential fit of the fluorescence decay (see Figures S10–S15 in the SI).

365 To further ascertain the CT character of the amino-substituted dyes, we calculated
366 the excited-state properties in Franck-Condon region of the benzothiazole derivatives
367 in three additional solvents: MCH, DMF and THF. The results of those calculations
368 together with the corresponding EDD plots are presented in Table S3 in the SI. As can
369 be seen, the above-described trends (obtained in chloroform) pertain, e.g., the S_0 → S_1
370 transition is associated with a much smaller μ_{ES} - μ_{GS} in the R=H (not exceeding 3 D)
371 than in the R=NMe₂ dye (larger than 5.8 D). The EDD plots also tend to confirm the

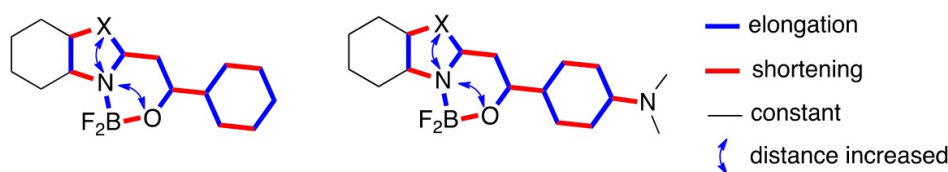
Table 5: Electron density difference plots and related electron transition parameters. All results were obtained at B3LYP/aug-cc-pVDZ level of theory for chloroform solution. Blue (red) color marks electron density depletion (gain) upon photon absorption. The contour value was set to 0.002 au.

Struct.		EDD plots	d_{CT}	q_{CT}	$\mu_{ES} - \mu_{GS}$
X	R		[Å]	[e]	[D]
NMe	H		2.310	0.427	4.734
O	H		2.101	0.430	4.339
S	H		1.539	0.407	3.007
NMe	NMe ₂		2.725	0.504	6.595
O	NMe ₂		2.713	0.502	6.537
S	NMe ₂		2.751	0.500	6.612

372 CT nature of $S_0 \rightarrow S_1$ transition of the R=NMe₂ derivatives: with density variations in
 373 the R=NMe₂ derivative showing a clear CT from the *p*-NMe₂-phenyl moiety (donor) to
 374 the BF₂-bearing moiety (acceptor).

375 To further characterize the first excited state beyond the Franck-Condon region, we
 376 have optimized the excited-state geometries of all compounds using TD-DFT. Let us first
 377 discuss the changes in bond lengths between the two electronic states. The complete set
 378 of data can be found in Table S2 in the SI. We focus our analysis on the geometrical
 379 changes, as given by $\Delta_{\text{bond}}^{\text{EG}} = \text{bond}^{\text{ES}} - \text{bond}^{\text{GS}}$. A graphical representation of the general
 380 variations of geometries can be found in Scheme 2. First, based on the comparison of

381 the sum of absolute changes of bond lengths in the series, it appears that the $S_0 \rightarrow S_1$
 382 excitation induces stronger effects for unsubstituted derivatives ($R=H$) than that for
 383 their substituted analogues ($R=NMe_2$). Indeed, the total variations, $\Sigma \Delta_{\text{bond}}^{\text{EG}}$, are equal
 384 to 1.249 Å and 1.157 Å, for the $R=H$ and $R=NMe_2$ series, respectively. This holds for the
 385 bonds belonging to the heterocyclic part of the structures, confirming that the excitation
 386 causes more dramatic changes in geometry for $R=H$, which is detrimental for emission
 387 yields. In contrast, except for the C11-C14 distance, the opposite trends are observed for
 388 1,4-phenylene ring moieties. This can be easily explained by the presence of NMe_2 donor
 389 which strongly affects the electron density distribution thus also the geometry of the
 390 $R=NMe_2$ dyes (See Figure S2 in the SI). Second, most of the computed changes in bond
 391 distances follow a $N \rightarrow O \rightarrow S$ ranking, e.g., for the C10-C11 bond, the excitation-induced
 392 changes are maximal for $X=S$ derivatives and minimal for their $X=NMe$ counterparts.
 393 In contrast, for the C9-N1 bond distance the above trend is reversed in both dye series
 394 (See Figure S1 in the SI). Third, for the side phenyl rings, the expected *p*-quinoid form
 395 ($=C(-CH=CH-)_2C=$) is favored upon excitation. This can be deduced based on the
 396 fact that two, out of six, ring bonds are shorter, while four of them are elongated when
 397 passing from the GS to the ES geometry (see Scheme 2). Interestingly, somewhat similar
 398 trends are observed for five-membered ring, i.e., N1-C2 and C2-X3 bonds become longer,
 399 while X3-C4 and C9-N1 distances become shorter upon excitation.

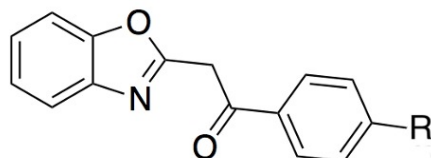


Scheme 2: Schematic representation of geometry changes upon excitation in $R=H$ and $R=NMe_2$ dyes.

400 4. Conclusions

401 We have investigated the influence of heteroatom (X=O, S, and NMe) substitution
402 in five-membered heterocyclic ring on the photophysical properties of novel BF₂ com-
403 plexes containing or not a dimethylamino group (R=NMe₂). The experimental results
404 showed that the photophysical properties of the molecules bearing an electron-donating
405 group are substantially different from these observed for unsubstituted analogues, which
406 follows previous findings of our groups [2; 50; 82]. For instance, the NMe→O heteroatom
407 replacement has a negligible impact on the absorption and emission properties of R=H
408 derivatives, but induces significant red-shifts accompanied by changes of the relative in-
409 tensities of absorption/emission shoulders for R=NMe₂ compounds. More pronounced
410 changes stem from the NMe→S substitution, i.e., both R=H and R=NMe₂ optical bands
411 are substantially redshifted. It is noteworthy that all R=NMe₂ derivatives exhibit fluo-
412 rescence quantum yields significantly higher (up to one order of magnitude) than their
413 unsubstituted counterparts. The experimental data were supported by the quantum
414 chemistry calculations, which not only reproduced the experimental trends but also con-
415 tributed to the understanding of electronic structure and excited-state properties: i)
416 the different photophysical properties of the R=NMe₂ fluorophores likely result from the
417 more pronounced CT character of their $S_0 \rightarrow S_1$ transition, as evidenced by both the large
418 inhomogeneous broadening of the absorption spectra obtained with the PERI-CC2 sim-
419 ulations and the dipole moment differences obtained at various levels of theories; ii) the
420 difference between absorption band topologies of R=H and R=NMe₂ have their roots in
421 the CT nature of the latter derivatives, that washes out the impact of vibronic couplings,
422 as PERI-CC2 calculations show that only one electronic state contributes to the overall
423 visible absorption band; and iii) the enhancement of fluorescence quantum yield observed
424 for compounds with R=NMe₂ can be linked to stabilization of a more planar structure,
425 both in the ground and the excited electronic states.

426 **5. Experimental Section**



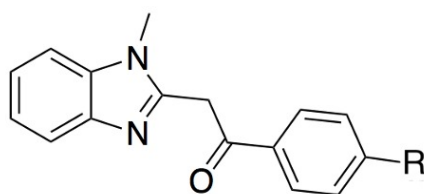
R = NMe₂, H

427 In general, 2-phenacylbenzoxazoles can be obtained in the condensation of 2-amino-
428 phenol and 3,3-dialkoxy-3,3-dimercapto-1-phenylprop-2-en-1-ones [125; 126] or alkyl ben-
429 zoylacetates [127]. These compounds were also conveniently prepared by subtraction of
430 one of the methyl protons in 2-methylbenzoxazole and treatment of the formed carban-
431 ion with acylating agent such as benzoic acid ester or benzoyl chloride [81; 128–137].
432 All compounds discussed in the present paper were obtained in the two-step synthesis
433 starting from 2-methylbenzoxazole and substituted benzoyl chlorides as before [133]. It
434 is worth underscoring the tautomeric equilibrium exists in these compounds.

435 2-Phenacylbenzoxazole - White solid, yield 59%, Mp 94–96°C; 94–96°C [81], 88–
436 88.5°C [126], 88–88.5°C [128], 88°C [129], 90–91°C [130], 97–98°C [125], and 93.5–
437 94.5°C [131]. In CDCl₃ solution 2-phenacylbenzoxazole (ketimine tautomeric form) is in
438 equilibrium with (Z)-2-(1,3-benzoxazol-2-yl)-1-phenylethenol (enolimine form). ¹H NMR
439 (CDCl₃ from TMS) δ: 12.50 (br s, 1H), 8.06 (m, 1H), 7.89 (m, 3H), 7.73 (m, 1H), 7.62
440 (m, 2H), 7.50 (m, 3H), 7.46 (m, 4H), 7.33 (m, 2H), 7.29 (m, 1H), 6.21 (s, 1H), 4.64
441 (s, 1H). ¹³C NMR δ: 192.4, 166.3, 165.74, 160.4, 151.3, 148.8, 141.3, 139.9, 135.8, 134.1,
442 133.9, 130.6, 128.9, 128.6, 128.6, 125.9, 125.0, 124.6, 124.3, 124.1, 120.0, 117.9, 110.6,
443 110.2, 83.7, 39.6. ¹⁵N NMR (CDCl₃ from MeNO₂) δ: -134.4, -164.1. C₁₅H₁₁NO₂ Calcd.
444 C 75.94, H 4.67, N 5.90; Found C 75.87, H 4.75, N 5.83.

445 2-(1,3-benzoxazol-2-yl)-1-[4-(dimethylamino)phenyl]ethanone - White solid, yield: 73%,
446 Mp 199–200.4°C; 197–198°C [81]. In CDCl₃ solution 2-(1,3-benzoxazol-2-yl)-1-[4-(dimethyl-
447 amino)phenyl]ethanone (ketimine tautomeric form) is in equilibrium with (Z)-2-(1,3-

448 benzoxazol-2-yl)-1-[4-(dimethylamino)phenyl]ethenol (enolimine form). ¹H NMR (CDCl₃
449 from TMS) δ: 7.96 (m, 2H), 7.72 (m, 1H), 7.50 (m, 1H), 7.29 (m, 2H), 6.68 (m, 2H),
450 6.05 (s, 1H, signal of low intensity coming from low amount of the enolimine form), 4.53
451 (s, 1H), 3.05 (s, 6H). ¹³C NMR δ: 190.0, 166.7, 161.6, 153.9, 151.3, 141.5, 131.0, 127.3,
452 124.8, 124.4, 124.2, 123.7, 123.4, 119.9, 111.5, 110.8, 110.6, 80.4, 40.0, 39.1, ¹⁵N NMR
453 (CDCl₃ from MeNO₂) δ: -135.6, -322.9. C₁₇H₁₆N₂O₂, Calcd. C 72.84, H 5.75, N 9.99.
454 Found C 72.66, H 5.88, N 9.86.



R = NMe₂, H

455 Some of 1-methyl-2-phenacylbenzimidazoles were synthesized according to reaction
456 of benzoyl substituted mercaptals with *N*-methyl-*o*-phenylenediamine [138; 139]. Afore-
457 mentioned synthesis, as well as other earlier described in the literature [125; 140], are
458 characterized by low yield, therefore 1-methyl-2-phenacylbenzimidazole were prepared by
459 treating 1,2-dimethylbenzimidazole with benzoyl chloride in the presence of triethylamine
460 followed by thermal decomposition of formed 2-(1-methyl-1*H*-benzo[*d*]imidazol-2-yl)-1-
461 phenylvinyl benzoate. Thus, benzoyl chloride (8 mmol) was added at once to the mix-
462 ture of 1,2-dimethylbenzimidazole (0.29 g, 2 mmol), triethylamine (0.81 g, 8 mmol) and
463 diglyme (10 mL) and the resulted mixture was heated (steam bath) and stirred overnight.
464 Addition of water (6 mL) precipitated the byproduct. Solution of morpholine (0.52 g,
465 6 mmol) in methanol (3 mL) was added to crude 2-(1-methyl-1*H*-benzo[*d*]imidazol-2-yl)-
466 1-phenylvinyl benzoate and the resulted mixture was refluxed for 5 min. Reaction was
467 quenched by addition of water (3 mL) and the precipitated solid product was recrystal-
468 lized from ethanol.

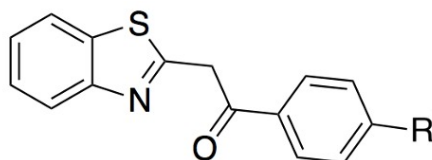
469 1-Methyl-2-phenacylbenzimidazole - Yellow solid, yield 40%, Mp 134–135.5°C; 119–

470 121°C (plates) and 149–152°C (needles) [49], 150–151°C and 134–134.5°C [139], 150–
471 152°C [125; 140], and 150–151.5°C [128; 141]. In CDCl₃ solution 1-methyl-2-phenacylbenz-
472 imidazole (ketimine tautomeric form) is in equilibrium with (Z)-2-(1-methyl-1*H*-benzi-
473 midazol-2-yl)-1-phenylethenol (enolimine form). ¹H NMR (CDCl₃ from TMS) δ: 14.04
474 (br s, 1H), 8.13 (d, 2H, ³J_{H,H}=7.32 Hz), 7.93 (m, 2H), 7.74 (m, 1H), 7.61 (m, 1H), 7.50
475 (m, 2H), 7.43 (m, 4H), 7.33 (m, 1H), 7.28 (m, 1H), 7.23 (m, 3H), 5.91 (s, 1H), 4.70
476 (s, 2H), 3.76 (s, 3H), 3.67 (s, 3H). ¹³C NMR δ: 194.0, 174.8, 154.4, 148.6, 138.4, 134.9,
477 134.8, 134.0, 133.14, 130.11, 129.9, 128.93, 128.87, 128.83, 128.3, 127.3, 126.2, 124.3,
478 122.9, 122.8, 122.7, 122.3, 122.2, 119.3, 113.9, 110.6, 109.4, 108.3, 77.0, 39.1, 30.5, 29.1.
479 ¹⁵N NMR (CDCl₃ from MeNO₂) δ: -137.4, -210.4, -233.3, -253.5. C₁₆H₁₄N₂O, Calcd.
480 C 76.78, H 5.64, N 11.19. Found C 76.85, H 5.74, N 11.03.

481 A slightly modified procedure [139] was used to prepare 1-[4-(dimethylamino)phenyl]-
482 2-(1-methyl-1*H*-benzimidazol-2-yl)ethanone. A mixture of 1,2-dimethylbenzimidazole
483 (0.29 g, 2 mmol), ethyl 4-(dimethylamino)benzoate (0.39 g, 2 mmol), dry benzene (10 mL),
484 dimethylformamide (0.5 mL) and sodium hydride (0.15 g, 60% suspension in mineral oil)
485 was refluxed and stirred magnetically overnight. The reaction was quenched by addition
486 of water (15 mL) and the resulted mixture was extracted with ethyl acetate (20 mL). The
487 organic layer was subsequently washed with water (2 x 10 mL) and brine (2 x 10 mL) and
488 dried with sodium sulfate. Solid impurities were filtered off, the filtrate was concentrated
489 on the rotary evaporator. The obtained solid was recrystallized from ethanol.

490 1-[4-(dimethylamino)phenyl]-2-(1-methyl-1*H*-benzimidazol-2-yl)ethanone - Yellow solid,
491 yield 36%, Mp 228–230°C, and 228–230°C [49]. In CDCl₃ solution 1-[4-(dimethylamino)-
492 phenyl]-2-(1-methyl-1*H*-benzimidazol-2-yl)ethanone (ketimine tautomeric form) is in equi-
493 librium with (Z)-1-[4-(dimethylamino)phenyl]-2-(1-methyl-1*H*-benzimidazol-2-yl)ethenol
494 (enolimine form). ¹H NMR (CDCl₃ from TMS) δ: 8.02 (m, 2H), 7.68 (d, 1H, ³J_{H,H}=8.80 Hz),
495 7.74 (m, 2H), 7.30 (m, 1H), 7.24 (m, 1H), 7.18 (m, 2H), 6.73 (m, 4H), 6.66 (m, 2H), 5.81
496 (s, 1H), 4.61 (s, 2H), 3.78 (s, 6H), 3.03 (s, 6H), 3.01 (s, 6H). ¹³C NMR δ: 191.7, 170.8,
497 153.8, 153.5, 149.8, 142.2, 136.1, 131.9, 131.2, 127.5, 123.7, 122.4, 122.3, 122.0, 119.2,

498 116.8, 111.4, 110.73, 110.67, 110.4, 109.3, 74.9, 40.1, 40.0, 38.8, 30.5. ¹⁵N NMR (CDCl₃
499 from MeNO₂) δ: -136.8, -233.8, -317.3. C₁₈H₁₉N₃O, Calcd. C 73.69, H 6.53, N 14.32.
500 Found C 73.78, H 6.63, N 14.23.

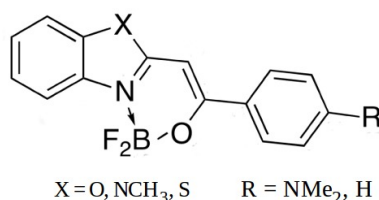


R = NMe₂, H

501 2-Methylbenzothiazole (2.5 g, 16.7 mmol) was added to a suspension of NaH (2 g,
502 50 mmol, 60% suspension in oil) in dry THF (15 mL) stirred at room temperature for 2 h.
503 After that time methyl benzoate (3.27 g, 21.8 mmol) or ethyl 4-(dimethylamino)benzoate
504 (4.21 g, 21.8 mmol) was added, and the resulting mixture was heated at reflux and stirred
505 magnetically overnight. After cooling down to room temperature, 2 M HCl aq. was slowly
506 added, and the yellow precipitate was filtered and washed with water. Resulting solid was
507 purified by column chromatography (SiO₂, DMC) [142–144]. Other methods of synthesis
508 of 2-phenacylbenzothiazoles are reported in the literature [125; 128; 134; 136; 137; 145–
509 147].

510 2-phenacylbenzothiazole - yellow solid, yield 69%, Mp 110.5–112.5°C, 113.5–114.5°C
511 [134], 110°C [129], 114°C [125], 113–114°C [126], 110–111°C [128], and 116–117°C [142].
512 In CDCl₃ solution 2-phenacylbenzothiazole (ketimine tautomeric form) is in equilibrium
513 with (Z)-2-(1,3-benzothiazol-2-yl)-1-phenylethenol (enolimine form). ¹H NMR (CDCl₃
514 from TMS) δ: 13.81 (br s, 1H), 8.09 (d, 2H, ³J_{H,H}=7.36 Hz), 8.03 (m, 1H), 7.88 (m, 2H),
515 7.80 (m, 2H), 7.59 (m, 4H), 7.52 (m, 4H), 7.39 (m, 1H), 7.30 (m, 1H), 6.38 (s, 1H), 4.85
516 (s, 1H). ¹³C NMR δ: 194.0, 168.1, 165.6, 163.8, 152.3, 150.4, 135.8, 135.2, 134.8, 133.9,
517 131.4, 130.4, 130.0, 129.1, 128.9, 128.7, 128.5, 127.5, 126.5, 126.2, 125.9, 125.2, 124.2,
518 122.8, 122.4, 121.6, 121.4, 120.0, 90.9, 43.7. ¹⁵N NMR (CDCl₃ from MeNO₂) δ: -120.0.
519 C₁₅H₁₁NOS, Calcd. C 71.12, H 4.38, N 5.53. Found C 71.20, H 4.51, N 5.42.

520 2-(1,3-benzothiazol-2-yl)-1-[4-(dimethylamino)phenyl]ethanone - yellow solid, yield
 521 77%, Mp 207–208°C. ¹H NMR (CDCl₃ from TMS) δ: 7.99 (m, 3H), 7.86 (d, 1H,
 522 ³J_{H,H}=8.0 Hz), 7.45 (m, 1H), 7.36 (m, 1H), 6.67 (d, 2H, ³J_{H,H}=8.0 Hz), 4.75 (s, 2H),
 523 3.07 (s, 6H). ¹³C NMR δ: 191.8, 165.1, 153.8, 152.6, 136.0, 131.1, 127.5, 126.3, 125.8,
 524 124.9, 123.6, 123.6, 122.7, 121.5, 121.3, 110.8, 88.4, 43.3, 40.0. ¹⁵N NMR (CDCl₃ from
 525 MeNO₂) δ: -67.8, -317.1. C₁₇H₁₆N₂OS, Calcd. C 68.89, H 5.44, N 9.45. Found C 68.95,
 H 5.57, N 9.29. The complexes were prepared based on a literature protocol [82]. For



526

527 their purification DCM was used as eluent in column chromatography (SiO₂).

528 1,1-difluoro-5-methyl-3-phenyl-1,5-dihydrobenzo[4,5]imidazo[1,2-*c*][1,3,2]oxazaborinin-
 529 10-ium-1-uide (**X=NMe**, **R=H**) - White solid, yield 36%, Mp 255.6–256.7°C. ¹H NMR
 530 (DMSO-*d*₆ from TMS) δ: 8.09 (m, 2H), 7.77 (m, 1H), 7.68 (m, 1H) 7.56 (m, 3H), 7.44
 531 (m, 2H), 7.05 (s, 1H), 3.98 (s, 3H). ¹¹B NMR (DMSO-*d*₆ from BF₃·Et₂O) δ: 1.66 (t).
 532 ¹³C NMR δ: 164.8, 150.4, 134.4, 133.8, 132.0, 131.7, 129.2, 126.9, 125.1, 124.8, 114.3,
 533 111.8, 81.8, 30.5. ¹⁵N NMR (DMSO-*d*₆ from MeNO₂) δ: -218.76, -242.04. ¹⁹F NMR
 534 (DMSO-*d*₆ from CFCl₃) δ: -134.14. C₁₆H₁₃BF₂N₂O, Calcd. C 64.47, H 4.40, N 9.40;
 535 Found C 64.53, H 4.46, N 9.48.

536 3-(4-(dimethylamino)phenyl)-1,1-difluoro-5-methyl-1,5-dihydrobenzo[4,5]imidazo[1,2-
 537 *c*][1,3,2]oxazaborinin-10-ium-1-uide (**X=NMe**, **R=NMe₂**) - Yellow solid, yield 39%,
 538 Mp 282–283.4°C. ¹H NMR (DMSO-*d*₆ from TMS) δ: 7.97 (d, 2H, ³J_{H,H}=9.04 Hz), 7.74
 539 (m, 1H), 7.65 (m, 1H) 7.46 (m, 2H), 6.85 (d, 2H, ³J_{H,H}=9.12 Hz), 6.79 (s, 1H), 3.96
 540 (s, 3H), 3.09 (s, 6H). ¹¹B NMR (DMSO-*d*₆ from BF₃·Et₂O) δ: 1.59 (t). ¹³C NMR δ:
 541 166.1, 152.7 151.2, 133.8, 131.9, 128.5, 124.6, 124.2, 120.8, 113.8, 111.7, 111.3, 77.9,
 542 ca. 40.64-39.36 (overlapped with solvent), 30.23. ¹⁵N NMR (DMSO-*d*₆ from MeNO₂) δ:

543 -211.89, -245.63, -319.77. ¹⁹F NMR (DMSO-d₆ from CFCl₃) δ: -134.64. C₁₈H₁₈BF₂N₃O,
544 Calcd. C 63.37, H 5.32, N 12.32; Found C 63.30, H 5.44, N 12.30.

545 1,1-difluoro-3-phenyl-1*H*-benzo[4,5]oxazolo[3,2-*c*][1,3,2]oxazaborinin-10-ium-1-uide
546 (**X=O**, **R=H**) - Yellowish-green solid, yield 38%, Mp 239.2–240.8°C. ¹H NMR (DMSO-
547 d₆ from TMS) δ: 8.12 (m, 2H), 7.94 (m, 1H), 7.72 (m, 1H) 7.65 (m, 1H), 7.59 (m, 4H),
548 7.55 (d, 1H, ³J_{H,H}=1.64 Hz), 7.22 (s, 1H). ¹¹B NMR (DMSO-d₆ from BF₃·Et₂O) δ: 1.85,
549 (t). ¹³C NMR δ: 170.8, 165.1, 148.5, 133.1, 130.1, 129.5, 127.5, 126.9, 126.4, 114.9, 112.5,
550 82.1. ¹⁵N NMR (DMSO-d₆ from MeNO₂) δ: -213.54. ¹⁹F NMR (DMSO-d₆ from CFCl₃)
551 δ: -135.07. C₁₅H₁₀BF₂NO₂, Calcd. C 63.20, H 3.54, N 4.91; Found C 63.25, H 3.49,
552 N 4.83.

553 3-(4-(dimethylamino)phenyl)-1,1-difluoro-1*H*-benzo[4,5]oxazolo[3,2-*c*][1,3,2]oxazaborinin-
554 10-ium-1-uide (**X=O**, **R=NMe₂**) - Orange solid, yield 41%, Mp 298–300°C. ¹H NMR
555 (DMSO-d₆ from TMS) δ: 7.96 (d, 2H, ³J_{H,H}=9.12 Hz), 7.85 (d, 1H, ³J_{H,H}=7.36 Hz), 7.61
556 (d, 1H, ³J_{H,H}=7.64 Hz), 7.50 (m, 2H), 6.89 (s, 1H), 6.81 (d, 2H, ³J_{H,H}=9.16 Hz), 3.07
557 (s, 6H). ¹¹B NMR (DMSO-d₆ from BF₃·Et₂O) δ: 1.79, (t). ¹³C NMR δ: 172.1 153.7,
558 152.4, 148.2, 130.6, 129.6, 127.0, 125.9, 119.1, 114.2, 112.1, 111.8, 77.7, ca. 40.61-39.35
559 (overlapped with solvent). ¹⁵N NMR (DMSO-d₆ from MeNO₂) δ: -313.97. ¹⁹F NMR
560 (DMSO-d₆ from CFCl₃) δ: -133.19. C₁₇H₁₅BF₂N₂O₂, Calcd. C 62.23, H 4.61, N 8.54;
561 Found C 62.14, H 4.64, N 8.39.

562 1,1-difluoro-3-phenyl-1*H*-benzo[4,5]thiazolo[3,2-*c*][1,3,2]oxazaborinin-10-ium-1-uide
563 (**X=S**, **R=H**) - Yellow solid, yield 43% Mp 244.5–245.7°C. ¹H NMR (DMSO-d₆ from
564 TMS) δ: 8.23 (d, 1H, ³J_{H,H}=8.0 Hz), 8.13 (m, 2H), 8.00 (d, 1H, ³J_{H,H}=8.16 Hz) 7.69
565 (m, 1H), 7.59 (m, 4H), 7.51 (s, 1H). ¹¹B NMR (DMSO-d₆ from BF₃·Et₂O) δ: 1.64 (t).
566 ¹³C NMR δ: 169.3, 164.9, 142.1, 133.1, 132.8, 129.5, 129.4, 128.9, 127.3, 126.6, 124.1,
567 117.8, 90.8. ¹⁵N NMR (DMSO-d₆ from MeNO₂) δ: -186.16. ¹⁹F NMR (DMSO-d₆ from
568 CFCl₃) δ: -132.16. C₁₅H₁₀BF₂NOS, Calcd. C 59.83, H 3.35, N 4.65. Found C 59.75,
569 H 3.43, N 4.54.

570 3-(4-(dimethylamino)phenyl)-1,1-difluoro-1*H*-benzo[4,5]thiazolo[3,2-*c*][1,3,2]oxazabor-

571 inin-10-ium-1-uide ($\mathbf{X}=\mathbf{S}$, $\mathbf{R}=\mathbf{NMe}_2$) - Yellow solid, yield 44%, Mp 280–283°C. ^1H NMR
572 (DMSO- d_6 from TMS) δ : 8.17 (d, 1H, $^3J_{\text{H,H}}=8.0$ Hz), 7.89 (m, 2H), 7.85 (s, 1H) 7.61
573 (m, 1H), 7.47 (m, 1H), 7.23 (s, 1H), 6.82 (d, 2H), 3.06 (s, 1H). ^{11}B NMR (DMSO- d_6 from
574 $\text{BF}_3\cdot\text{Et}_2\text{O}$) δ : 1.54 (t). ^{13}C NMR δ : 168.5, 166.5, 153.5, 142.3, 129.4, 128.5, 125.7, 123.8,
575 118.8, 117.1, 111.9, 87.6, ca. 40.60-39.35 (overlapped with solvent). ^{15}N NMR (DMSO-
576 d_6 from MeNO_2) δ : -194.22, -314.90. ^{19}F NMR (DMSO- d_6 from CFCl_3) δ : -133.09.
577 $\text{C}_{17}\text{H}_{15}\text{BF}_2\text{N}_2\text{OS}$, Calcd. C 59.32, H 4.39, N 8.14. Found C 59.43, H 4.45, N 8.06.

578 Acknowledgments

579 B.O. and A.M.G. thank the Polish National Science Centre (Grant No.
580 2017/26/M/ST5/00327). W.B. acknowledges the statutory activity subsidy from the
581 Polish Ministry of Science and Higher Education for the Faculty of Chemistry of Wrocław
582 University of Technology. The authors want to address special and warm gratitude
583 to Dr Robert Zaleśny from Faculty of Chemistry, Wrocław University of Science and
584 Technology for countless valuable discussions which helped to improve manuscript and
585 his kind and precious help with CC2 calculations. Authors are also very grateful to
586 Damian Plazuk from University of Łódź for recording fluorescence quantum yield with
587 the use of the integrating sphere. The calculations were performed at the Wrocław Center
588 for Networking and Supercomputing.

589 Supporting Informations

590 The Supporting Information is available on the Elsevier website. It contains fluo-
591 rescence decay curves, NMR spectra, Cartesian coordinates, computational results and
592 bond-lenghts analysis.

593 References

594 [1] I. Kaya, M. Yildirim, A. Avci, Synthesis and characterization of fluorescent polyphenol species de-
595 rived from methyl substituted aminopyridine based schiff bases: The effect of substituent position

- 596 on optical, electrical, electrochemical, and fluorescence properties, *Synth. Met.* 160 (9-10) (2010)
597 911–920.
- 598 [2] A. Zakrzewska, R. Zaleśny, E. Kolehmainen, B. Ośmiałowski, B. Jędrzejewska, H. Ågren,
599 M. Pietrzak, Substituent effects on the photophysical properties of fluorescent 2-
600 benzoylmethylenequinoline difluoroboranes: A combined experimental and quantum chemical
601 study, *Dyes Pigm.* 99 (2013) 957–965.
- 602 [3] K.-Y. Chen, H.-Y. Tsai, W.-C. Lin, H.-H. Chu, Y.-C. Weng, C.-C. Chan, Esipt fluorescent dyes
603 with adjustable optical properties: Substituent and conjugation effects, *J. Lumin.* 154 (2014)
604 168–177.
- 605 [4] T. Yoshida, T. Furuyama, M. Asai, N. Kobayashi, Fluorescence enhancement of tetraazaporphyrins
606 by the use of bulky substituent effects, *Chem. Lett.* 44 (8) (2015) 1056–1058.
- 607 [5] M.-S. Tsai, C.-L. Ou, C.-J. Tsai, Y.-C. Huang, Y.-C. Cheng, S.-S. Sun, J.-S. Yang, Fluorescence
608 enhancement of unconstrained gfp chromophore analogues based on the push-pull substituent
609 effect, *J. Org. Chem.* 82 (15) (2017) 8031–8039.
- 610 [6] D. Wang, X. Fan, S. Sun, S. Du, H. Li, J. Zhu, Y. Tang, M. Chang, Y. Xu, Substituent effect:
611 A new strategy to construct a ratiometric fluorescent probe for detection of Al^{3+} and imaging in
612 vivo, *Sens. Actuator B-Chem.* 264 (2018) 304–311.
- 613 [7] T. Uppal, X. Hu, F. Fronczek, S. Maschek, P. Bobadova-Parvanova, M. Vicente, Synthesis, com-
614 putational modeling, and properties of benzo-appended bodipys, *Chem. Eur. J.* 18 (13) (2012)
615 3893–3905.
- 616 [8] Y. Ni, W. Zeng, K.-W. Huang, J. Wu, Benzene-fused bodipys: synthesis and the impact of fusion
617 mode, *Chem. Commun.* 49 (12) (2013) 1217–1219.
- 618 [9] S.-I. Kato, T. Furuya, M. Nitani, N. Hasebe, Y. Ie, Y. Aso, T. Yoshihara, S. Tobita, Y. Naka-
619 mura, A series of π -extended thiadiazoles fused with electron-donating heteroaromatic moieties:
620 Synthesis, properties, and polymorphic crystals, *Chem. Eur. J.* 21 (7) (2015) 3115–3128.
- 621 [10] J. Golden, J. Facendola, D. Sylvinson, C. Baez, P. Djurovich, M. Thompson, Boron dipyriddy-
622 methene (dipyr) dyes: Shedding light on pyridine-based chromophores, *J. Org. Chem.* 82 (14)
623 (2017) 7215–7222.
- 624 [11] O. Kim, J. Jang, H. Kim, S. Han, G. Tsui, J. Joo, Synthesis of fluorescent indazoles by palladium-
625 catalyzed benzannulation of pyrazoles with alkynes, *Org. Lett.* 19 (6) (2017) 1450–1453.
- 626 [12] W.-Q. Zhang, K. Cheng, X. Yang, Q.-Y. Li, H. Zhang, Z. Ma, H. Lu, H. Wu, X.-J. Wang, A
627 benzothiadiazole-based fluorescent sensor for selective detection of oxalyl chloride and phosgene,
628 *Org. Chem. Front.* 4 (9) (2017) 1719–1725.
- 629 [13] G. Li, K.-J. Jiang, Y.-F. Li, S.-L. Li, L.-M. Yang, Efficient structural modification of
630 triphenylamine-based organic dyes for dye-sensitized solar cells, *J. Phys. Chem. C* 112 (30) (2008)

- 631 11591–11599.
- 632 [14] G. De Miguel, M. Wielopolski, D. Schuster, M. Fazio, O. Lee, C. Haley, A. Ortiz, L. Echegoyen,
633 T. Clark, D. Guldi, Triazole bridges as versatile linkers in electron donor-acceptor conjugates, *J.*
634 *Am. Chem. Soc.* 133 (33) (2011) 13036–13054.
- 635 [15] A. Fihey, A. Perrier, W. R. Browne, D. Jacquemin, Multiphotochromic molecular systems, *Chem.*
636 *Soc. Rev.* 44 (2015) 3719–3759.
- 637 [16] A. Grabarz, A. D. Laurent, B. Jędrzejewska, A. Zakrzewska, D. Jacquemin, B. Ośmiałowski, The
638 influence of the π -conjugated spacer on photophysical properties of difluoroboranyls derived from
639 amides carrying a donor group, *J. Org. Chem.* 81 (2016) 2280–2292.
- 640 [17] M. M. Alcaide, F. M. F. Santos, V. F. Pais, J. I. Carvalho, D. Collado, E. Pérez-Inestrosa, J. F.
641 Arteaga, F. Boscá, P. M. P. Gois, U. Pischel, Electronic and functional scope of boronic acid
642 derived salicylidenehydrazone (bashy) complexes as fluorescent dyes, *J. Org. Chem.* 82 (14) (2017)
643 7151–7158.
- 644 [18] C. Flors, I. Oesterling, T. Schnitzler, E. Fron, G. Schweitzer, M. Sliwa, A. Herrmann, M. van der
645 Auweraer, F. C. de Schryver, K. Müllen, J. Hofkens, Energy and electron transfer in ethynylene
646 bridged perylene diimide multichromophores, *J. Phys. Chem. C* 111 (12) (2007) 4861–4870.
- 647 [19] X. Lv, T. Li, Q. Wu, C. Yu, L. Jiao, E. Hao, Polybrominated bophy dyes: Synthesis, reactivity,
648 and properties, *J. Org. Chem.* 83 (3) (2018) 1134–1145.
- 649 [20] P. Wei, J.-X. Zhang, Z. Zhao, Y. Chen, X. He, M. Chen, J. Gong, H.-Y. Sung, I. Williams, J. Lam,
650 B. Tang, Multiple yet controllable photoswitching in a single aiegen system, *J. Am. Chem. Soc.*
651 140 (5) (2018) 1966–1975.
- 652 [21] X. Chen, T. Pradhan, F. Wang, J. Kim, J. Yoon, Fluorescent chemosensors based on spiroring-
653 opening of xanthenes and related derivatives, *Chem. Rev.* 112 (3) (2012) 1910–1956.
- 654 [22] I. Astakhova, J. Wengel, Interfacing click chemistry with automated oligonucleotide synthesis for
655 the preparation of fluorescent dna probes containing internal xanthene and cyanine dyes, *Chem.*
656 *Eur. J.* 19 (3) (2013) 1112–1122.
- 657 [23] A. Pandey, A. Kumar, S. Vishwakarma, K. Upadhyay, A highly specific 'turn-on' fluorescent
658 detection of mg^{2+} through a xanthene based fluorescent molecular probe, *RSC Adv.* 6 (8) (2016)
659 6724–6729.
- 660 [24] S. Ma, Y. Wang, M. She, S. Wang, Z. Yang, P. Liu, S. Zhang, J. Li, Design strategies and progress
661 on xanthene-based fluorescent probe for metal ions, *Reviews in Anal. Chem.* 36 (2).
- 662 [25] K. More, T.-H. Lim, S.-Y. Kim, J. Kang, K.-S. Inn, D.-J. Chang, Characteristics of new biore-
663 ductive fluorescent probes based on the xanthene fluorophore: Detection of nitroreductase and
664 imaging of hypoxic cells, *Dyes Pigm.* 151 (2018) 245–253.
- 665 [26] L. Yuan, W. Lin, K. Zheng, L. He, W. Huang, Far-red to near infrared analyte-responsive fluo-

- 666 rescent probes based on organic fluorophore platforms for fluorescence imaging, *Chem. Soc. Rev.*
667 42 (2) (2013) 622–661.
- 668 [27] G. Cheng, J. Fan, W. Sun, J. Cao, C. Hu, X. Peng, A near-infrared fluorescent probe for selective
669 detection of hclo based on se-sensitized aggregation of heptamethine cyanine dye, *Chem. Commun.*
670 50 (8) (2014) 1018–1020.
- 671 [28] J. Yin, Y. Kwon, D. Kim, D. Lee, G. Kim, Y. Hu, J.-H. Ryu, J. Yoon, Cyanine-based fluorescent
672 probe for highly selective detection of glutathione in cell cultures and live mouse tissues, *J. Am.*
673 *Chem. Soc.* 136 (14) (2014) 5351–5358.
- 674 [29] A. Nano, A. Boynton, J. Barton, A rhodium-cyanine fluorescent probe: Detection and signaling
675 of mismatches in dna, *J. Am. Chem. Soc.* 139 (48) (2017) 17301–17304.
- 676 [30] X. Wang, J. Lv, X. Yao, Y. Li, F. Huang, M. Li, J. Yang, X. Ruan, B. Tang, Screening and
677 investigation of a cyanine fluorescent probe for simultaneous sensing of glutathione and cysteine
678 under single excitation, *Chem. Commun.* 50 (97) (2014) 15439–15442.
- 679 [31] G. Ulrich, R. Ziessel, A. Harriman, The chemistry of fluorescent bodipy dyes: versatility unsur-
680 passed, *Angew. Chem. Int. Ed.* 47 (7) (2008) 1184–1201.
- 681 [32] N. Boens, V. Leen, W. Dehaen, Fluorescent indicators based on bodipy, *Chem. Soc. Rev.* 41 (3)
682 (2012) 1130–1172.
- 683 [33] Y. Ni, J. Wu, Far-red and near infrared bodipy dyes: synthesis and applications for fluorescent ph
684 probes and bio-imaging, *Org. Biomol. Chem.* 12 (23) (2014) 3774–3791.
- 685 [34] F. Wang, L. Zhou, C. Zhao, R. Wang, Q. Fei, S. Luo, Z. Guo, H. Tian, W.-H. Zhu, A dual-
686 response bodipy-based fluorescent probe for the discrimination of glutathione from cystein and
687 homocystein, *Chem. Sci.* 6 (4) (2015) 2584–2589.
- 688 [35] Q. Fei, M. Li, J. Chen, B. Shi, G. Xu, C. Zhao, X. Gu, Design of bodipy-based near-infrared
689 fluorescent probes for h₂s, *J. Photochem. Photobiol. A* 355 (2018) 305–310.
- 690 [36] H. Jung, P. Kwon, J. Lee, J. Kim, C. Hong, J. Kim, S. Yan, J. Lee, J. Lee, T. Joo, J. Kim,
691 Coumarin-derived cu²⁺-selective fluorescence sensor: Synthesis, mechanisms, and applications in
692 living cells, *J. Am. Chem. Soc.* 131 (5) (2009) 2008–2012.
- 693 [37] H. Jung, K. Ko, G.-H. Kim, A.-R. Lee, Y.-C. Na, C. Kang, J. Lee, J. Kim, Coumarin-based
694 thiol chemosensor: Synthesis, turn-on mechanism, and its biological application, *Org. Lett.* 13 (6)
695 (2011) 1498–1501.
- 696 [38] J. Li, C.-F. Zhang, S.-H. Yang, W.-C. Yang, G.-F. Yang, A coumarin-based fluorescent probe for
697 selective and sensitive detection of thiophenols and its application, *Anal. Chem.* 86 (6) (2014)
698 3037–3042.
- 699 [39] V. Gupta, N. Mergu, L. Kumawat, A. Singh, Selective naked-eye detection of magnesium (ii) ions
700 using a coumarin-derived fluorescent probe, *Sens. Actuator B-Chem.* 207 (2015) 216–223.

- 701 [40] L. Wang, W. Li, W. Zhi, D. Ye, Y. Wang, L. Ni, X. Bao, A rapid-responsive fluorescent probe
702 based on coumarin for selective sensing of sulfite in aqueous solution and its bioimaging by turn-on
703 fluorescence signal, *Dyes Pigm.* 147 (2017) 357–363.
- 704 [41] R. Ziessel, G. Ulrich, A. Harriman, The chemistry of bodipy: A new *El Dorado* for fluorescence
705 tools, *New J. Chem.* 31 (2007) 496–501.
- 706 [42] M. A. Potopnyk, R. Lytvyn, Y. Danyliv, M. Ceborska, O. Bezikonnyi, D. Volyniuk, J. V. Gražule-
707 vičius, N, σ π -conjugated 4-substituted 1,3-thiazole bf_2 complexes: Synthesis and photophysical
708 properties, *J. Org. Chem.* 83 (3) (2018) 1095–1105.
- 709 [43] D. Frath, K. Benelhadj, M. Munch, J. Massue, G. Ulrich, Polyanils and polyboranils: Synthesis,
710 optical properties, and aggregation-induced emission, *J. Org. Chem.* 81 (20) (2016) 9658–9668.
- 711 [44] L. Weber, D. Eickhoff, A. Chrostowska, C. Darrigan, H.-G. Stammli, B. Neumann, Synthe-
712 sis, structure, and properties of luminescent diazaborole and indole systems, *Chem. Heterocycl.*
713 *Compd.* 53 (1) (2017) 54–65.
- 714 [45] K. Zhang, H. Zheng, C. Hua, M. Xin, J. Gao, Y. Li, Novel fluorescent n,o-chelated fluorine-
715 boron benzamide complexes containing thiadiazoles: Synthesis and fluorescence characteristics,
716 *Tetrahedron* 74 (2018) 4161–4167.
- 717 [46] C. Yu, E. Hao, T. Li, J. Wang, W. Sheng, Y. Wei, X. Mu, L. Jiao, Dipyrrolylquinoxaline difluo-
718 roborates with intense red solid-state fluorescence, *Dalton Trans.* 44 (2015) 13897–13905.
- 719 [47] G. Ulrich, S. Goeb, A. De Nicola, P. Retailleau, R. Ziessel, Chemistry at boron: Synthesis and
720 properties of red to near-ir fluorescent dyes based on boron-substituted diisindolomethene frame-
721 works, *J. Org. Chem.* 76 (11) (2011) 4489–4505.
- 722 [48] Y. Ni, W. Zeng, K.-W. Huang, J. Wu, Benzene-fused bodipys: synthesis and the impact of fusion
723 mode, *Chem. Commun.* 49 (2013) 1217–1219.
- 724 [49] A. Skotnicka, P. Czeleń, R. Gawinecki, Tautomeric equilibria in solutions of 1-methyl-2-
725 phenacylbenzimidazoles, *J. Mol. Struct.* 1134 (2017) 546–551.
- 726 [50] A. M. Grabarz, B. Jędrzejewska, A. Zakrzewska, R. Zaleśny, A. D. Laurent, D. Jacquemin,
727 B. Ośmiałowski, Photophysical properties of phenacylphenanthridine difluoroboranyl: effect of
728 substituent and double benzannulation, *J. Org. Chem.* 82 (3) (2017) 1529–1537.
- 729 [51] W. Sheng, J. Cui, Z. Ruan, L. Yan, Q. Wu, C. Yu, Y. Wei, E. Hao, L. Jiao, [a]-phenanthrene-fused
730 bf_2 azadipyrromethene (azabodipy) dyes as bright near-infrared fluorophores, *J. Org. Chem.* 82
731 (2017) 10341–10349.
- 732 [52] A. B. Descalzo, H.-J. Xu, Z. Shen, K. Rurack, Influence of the meso-substituent on strongly red
733 emitting phenanthrene-fused boron-dipyrromethene (bodipy) fluorophores with a propeller-like
734 conformation, *J. Photochem. Photobiol. A* 352 (2018) 98–105.
- 735 [53] X.-D. Jiang, X. Liu, T. Fang, C. Sun, L. Xiao, Synthesis and photophysical properties of long wave-

- length absorbing bodipy/aza-bodipy bearing a five-membered ring, *Tetrahedron Lett.* 59 (2018) 546–549.
- [54] W. Zhao, E. Carreira, Conformationally restricted aza-bodipy: Highly fluorescent, stable near-infrared absorbing dyes, *Chem. Eur. J.* 12 (27) (2006) 7254–7263.
- [55] R. Gresser, M. Hummert, H. Hartmann, K. Leo, M. Riede, Synthesis and characterization of near-infrared absorbing benzannulated aza-bodipy dyes, *Chem. Eur. J.* 17 (10) (2011) 2939–2947.
- [56] J. Min, T. Ameri, R. Gresser, M. Lorenz-Rothe, D. Baran, A. Troeger, V. Sgobba, K. Leo, M. Riede, D. Guldi, C. Brabec, Two similar near-infrared (ir) absorbing benzannulated aza-bodipy dyes as near-ir sensitizers for ternary solar cells, *ACS Appl. Mater. Interfaces* 5 (12) (2013) 5609–5616.
- [57] A. Diaz-Moscoco, E. Emond, D. Hughes, G. Tizzard, S. Coles, A. Cammidge, Synthesis of a class of core-modified aza-bodipy derivatives, *J. Org. Chem.* 79 (18) (2014) 8932–8936.
- [58] J. Karlsson, A. Harriman, Origin of the red-shifted optical spectra recorded for aza-bodipy dyes, *J. Phys. Chem. A* 120 (16) (2016) 2537–2546.
- [59] D. Frath, S. Azizi, G. Ulrich, P. Retailleau, R. Ziessel, Facile synthesis of highly fluorescent boranil complexes, *Org. Lett.* 13 (13) (2011) 3414–3417.
- [60] D. Frath, S. Azizi, G. Ulrich, R. Ziessel, Chemistry on boranils: An entry to functionalized fluorescent dyes, *Org. Lett.* 14 (18) (2012) 4774–4777.
- [61] G. N. Lipunova, E. V. Nosova, V. N. Charushin, O. N. Chupakhin, Boron(III) complexes with n,n'- and n,o-heterocyclic ligands: Synthesis and spectroscopic properties, *Comments Inorg. Chem.* 36 (5) (2016) 245–303.
- [62] M. Urban, K. Durka, P. Jankowski, J. Serwatowski, S. Luliński, Highly fluorescent red-light emitting bis(boranils) based on naphthalene backbone, *J. Org. Chem.* 82 (15) (2017) 8234–8241.
- [63] J. Massue, D. Frath, G. Ulrich, P. Retailleau, R. Ziessel, Synthesis of luminescent 2-(2'-hydroxyphenyl)benzoxazole (hbo) borate complexes, *Org. Lett.* 14 (1) (2012) 230–233.
- [64] J. Massue, G. Ulrich, R. Ziessel, Effect of 3,5-disubstitution on the optical properties of luminescent 2-(2'-hydroxyphenyl)benzoxazoles and their borate complexes, *Eur. J. Org. Chem.* (25) (2013) 5701–5709.
- [65] K. Benelhadj, J. Massue, P. Retailleau, S. Chibani, B. Le Guennic, D. Jacquemin, R. Ziessel, G. Ulrich, Solution- and solid-state luminescent borate complexes based on a substituted π -conjugated 2-(6'-hydroxy-5'-benzofuryl) scaffold, *Eur. J. Org. Chem.* (32) (2014) 7156–7164.
- [66] S. Xu, R. E. Evans, T. Liu, G. Zhang, J. N. Demas, C. O. Trindle, C. L. Fraser, Aromatic difluoroboron β -diketonate complexes: Effects of π -conjugation and media on optical properties, *Inorg. Chem.* 52 (7) (2013) 3597–3610.
- [67] A. D'Aleo, F. Fages, Boron difluoride complexes of 3-hydroxyflavone derivatives: efficient bioin-

- 771 spired dyes for solution and solid-state emission, *Photochem. Photobiol. Sci.* 12 (2013) 500–510.
- 772 [68] B. Štefane, F. Požgan, E. Kim, E. Choi, J.-C. Ribierre, J. W. Wu, M. Ponce-Vargas, B. L. Guennic,
773 D. Jacquemin, G. Canard, E. Zaborova, F. Fages, A. D'Aléo, Ethynylene-analogues of hemicur-
774 cuminoids: Synthesis and ground- and excited properties of their boron difluoride complexes, *Dyes*
775 *Pigm.* 141 (2017) 38–47.
- 776 [69] M. Santra, H. Moon, M.-H. Park, T.-W. Lee, Y. K. Kim, K. H. Ahn, Dramatic substituent effects
777 on the photoluminescence of boron complexes of 2-(benzothiazol-2-yl)phenols, *Chem. Eur. J.* 18
778 (2012) 9886–9893.
- 779 [70] U. Balijapalli, A. Joseph, S. Chinduluri, E. Shanmugam, K. Sathiyarayanan, Luminescent
780 tetrahydrodibenzo[a,i]phenanthridin-5-yl)phenol-boron complexes (borophenanthridines), *Dyes*
781 *Pigm.* 137 (2017) 182–190.
- 782 [71] Y. Kubota, M. Tsukamoto, K. Ohnishi, J. Jin, K. Funabiki, M. Matsui, Synthesis and fluorescence
783 properties of novel squarylium-boron complexes, *Org. Chem. Front.* 4 (2017) 1522–1527.
- 784 [72] J. Dobkowski, P. Wnuk, J. Buczyńska, M. Pszona, G. Orzanowska, D. Frath, G. Ulrich, J. Massue,
785 S. Mosquera-Vázquez, E. Vauthey, C. Radzewicz, R. Ziessel, J. Waluk, Substituent and solvent
786 effects on the excited state deactivation channels in anils and boranils, *Chem. Eur. J.* 21 (2014)
787 1312–1327.
- 788 [73] Y. Wu, W. Yuan, H. Ji, Y. Qin, J. Zhang, H. Li, Y. Li, Y. Wang, Y. Sun, W. Liu, New fluorescent
789 imidazo[1,2- α]pyridine-bodipy chromophores: Experimental and theoretical approaches, and cell
790 imaging exploration, *Dyes Pigm.* 142 (2017) 330–339.
- 791 [74] W. Chen, L. Zhu, Y. Hao, X. Yue, J. Gai, Q. Xiao, S. Huang, J. Sheng, X. Song, Detection of
792 thiophenol in buffer, in serum, on filter paper strip, and in living cells using a red-emitting amino
793 phenothiazine boranil based fluorescent probe with a large stokes shift, *Tetrahedron* 73 (31) (2017)
794 4529–4537.
- 795 [75] A. Loudet, K. Burgess, Bodipy dyes and their derivatives: Syntheses and spectroscopic properties,
796 *Chem. Rev.* 107 (11) (2007) 4891–4932.
- 797 [76] U. Balijapalli, K. Sathiyarayanan, Synthesis and optical properties of a series of green-light-
798 emitting 2-(4-phenylquinolin-2-yl)phenol-bf₂ complexes (boroquinols), *Eur. J. Org. Chem.* (23)
799 (2015) 5089–5098.
- 800 [77] S. Deshpande, H. Kumbhar, G. Shankarling, Photoswitchable conjugated assembly involving flu-
801 orescent boranil, *J. Lumin.* 179 (2016) 314–321.
- 802 [78] B. Jędrzejewska, A. Zakrzewska, G. Młostoń, Š. Budzák, K. Mroczyńska, A. M. Grabarz, M. A.
803 Kaczorowska, D. Jacquemin, B. Ośmiałowski, Synthesis and photophysical properties of novel
804 donor-acceptor n-(pyridin-2-yl)-substituted benzo(thio)amides and their difluoroboranyl deriva-
805 tives, *J. Phys. Chem. A* (24) (2016) 4116–4123.

- 806 [79] Z. Xu, G. Ding, G. Zhong, G. Xing, F. Li, W. Huang, H. Tian, Color tunable organic light-emitting
807 diodes using coumarin dopants, *Res. Chem. Intermed.* 34 (2) (2008) 249–256.
- 808 [80] V. S. Padalkar, A. Tathe, V. D. Gupta, V. S. Patil, K. Phatangare, N. Sekar, Synthesis and
809 photo-physical characteristics of esipt inspired 2-substituted benzimidazole, benzoxazole and ben-
810 zothiazole fluorescent derivatives, *J. Fluoresc.* 22 (1) (2012) 311–322.
- 811 [81] A. Skotnicka, E. Kolehmainen, P. Czeleń, A. Valkonen, R. Gawinecki, Synthesis and structural
812 characterization of substituted 2-phenacylbenzoxazoles, *Int. J. Mol. Sci.* 14 (3) (2013) 4444–4460.
- 813 [82] B. Ośmiałowski, A. Zakrzewska, B. Jędrzejewska, A. Grabarz, R. Zaleśny, W. Bartkowiak,
814 E. Kolehmainen, Influence of substituent and benzoannulation on photophysical properties of
815 1-benzoylmethyleneisoquinoline difluoroborates, *J. Org. Chem.* 80 (2015) 2072–2080.
- 816 [83] A. M. Brouwer, Standards for photoluminescence quantum yield measurements in solution (iupac
817 technical report), *Pure Appl. Chem.* 83 (2011) 2213–2011.
- 818 [84] J. Tomasi, M. Persico, Molecular interactions in solution: An overview of methods based on
819 continuous distributions of the solvent, *Chem. Rev.* 94 (7) (1994) 2027–2094.
- 820 [85] T. Schwabe, K. Sneskov, J. Haugaard Olsen, J. Kongsted, O. Christiansen, C. Hättig, Peri-cc2: A
821 polarizable embedded ri-cc2 method, *J. Chem. Theory Comput.* 8 (9) (2012) 3274–3283.
- 822 [86] C. M. Breneman, K. B. Wiberg, Determining atom-centered monopoles from molecular electro-
823 static potentials. the need for high sampling density in formamide conformational analysis, *J.*
824 *Comput. Chem.* 11 (1990) 361–373.
- 825 [87] J. Wang, R. M. Wolf, J. W. Caldwell, P. A. Kollman, D. A. Case, Development and testing of a
826 general amber force field, *J. Comput. Chem.* 25 (2004) 1157–1174.
- 827 [88] D. C. et al., AMBER 16, university of California, San Francisco (2016).
- 828 [89] TURBOMOLE V7.0 2015, a development of University of Karlsruhe and Forschungs-
829 szentrum Karlsruhe GmbH, 1989-2007, TURBOMOLE GmbH, since 2007; available from
830 <http://www.turbomole.com> (last accessed 01 apr. 17).
- 831 [90] M. J. Frisch, G. W. Trucks, H. B. Schlegel, G. E. Scuseria, M. A. Robb, J. R. Cheeseman,
832 G. Scalmani, V. Barone, B. Mennucci, G. A. Petersson, H. Nakatsuji, M. Caricato, X. Li, H. P.
833 Hratchian, A. F. Izmaylov, J. Bloino, G. Zheng, J. L. Sonnenberg, M. Hada, M. Ehara, K. Toyota,
834 R. Fukuda, J. Hasegawa, M. Ishida, T. Nakajima, Y. Honda, O. Kitao, H. Nakai, T. Vreven,
835 J. A. Montgomery, Jr., J. E. Peralta, F. Ogliaro, M. Bearpark, J. J. Heyd, E. Brothers, K. N.
836 Kudin, V. N. Staroverov, R. Kobayashi, J. Normand, K. Raghavachari, A. Rendell, J. C. Burant,
837 S. S. Iyengar, J. Tomasi, M. Cossi, N. Rega, J. M. Millam, M. Klene, J. E. Knox, J. B. Cross,
838 V. Bakken, C. Adamo, J. Jaramillo, R. Gomperts, R. E. Stratmann, O. Yazyev, A. J. Austin,
839 R. Cammi, C. Pomelli, J. W. Ochterski, R. L. Martin, K. Morokuma, V. G. Zakrzewski, G. A.
840 Voth, P. Salvador, J. J. Dannenberg, S. Dapprich, A. D. Daniels, Ö. Farkas, J. B. Foresman, J. V.

- 841 Ortiz, J. Cioslowski, D. J. Fox, Gaussian 2009, gaussian Inc. Wallingford CT 2009.
- 842 [91] A. D. Becke, Density-functional exchange-energy approximation with correct asymptotic behavior,
843 Phys. Rev. A 38 (1988) 3098–3100. doi:10.1103/PhysRevA.38.3098.
- 844 [92] C. Lee, W. Yang, R. G. Parr, Development of the colle-salveti correlation-energy formula into a
845 functional of the electron density, Phys. Rev. B 37 (1988) 785–789. doi:10.1103/PhysRevB.37.785.
846 URL <http://link.aps.org/doi/10.1103/PhysRevB.37.785>
- 847 [93] A. D. Becke, Density-functional thermochemistry. iii. the role of exact exchange, J. Chem. Phys.
848 98 (7) (1993) 5648–5652. arXiv:<http://dx.doi.org/10.1063/1.464913>, doi:10.1063/1.464913.
849 URL <http://dx.doi.org/10.1063/1.464913>
- 850 [94] C. Adamo, V. Barone, Toward reliable density functional methods without ad-
851 justable parameters: The pbe0 model, J. Chem. Phys. 110 (13) (1999) 6158–6170.
852 arXiv:<http://dx.doi.org/10.1063/1.478522>, doi:10.1063/1.478522.
853 URL <http://dx.doi.org/10.1063/1.478522>
- 854 [95] M. Ernzerhof, G. E. Scuseria, Assessment of the perdew-burke-ernzerhof exchange-correlation
855 functional, J. Chem. Phys. 110 (11) (1999) 5029–5036. arXiv:<http://dx.doi.org/10.1063/1.478401>,
856 doi:10.1063/1.478401.
857 URL <http://dx.doi.org/10.1063/1.478401>
- 858 [96] Y. Zhao, D. G. Truhlar, The m06 suite of density functionals for main group thermochemistry,
859 thermochemical kinetics, noncovalent interactions, excited states, and transition elements: two
860 new functionals and systematic testing of four m06-class functionals and 12 other functionals,
861 Theor. Chem. Acc. 120 (1) (2008) 215–241. doi:10.1007/s00214-007-0310-x.
862 URL <http://dx.doi.org/10.1007/s00214-007-0310-x>
- 863 [97] A. D. Becke, A new mixing of hartree-fock and local density-functional theories, J. Chem. Phys.
864 98 (2) (1993) 1372–1377. arXiv:<http://dx.doi.org/10.1063/1.464304>, doi:10.1063/1.464304.
865 URL <http://dx.doi.org/10.1063/1.464304>
- 866 [98] T. Yanai, D. P. Tew, N. C. Handy, A new hybrid exchange-correlation functional using
867 the coulomb-attenuating method (cam-b3lyp), Chem. Phys. Lett. 393 (1–3) (2004) 51–57.
868 doi:<http://dx.doi.org/10.1016/j.cplett.2004.06.011>.
869 URL <http://www.sciencedirect.com/science/article/pii/S0009261404008620>
- 870 [99] J.-D. Chai, M. Head-Gordon, Systematic optimization of long-range corrected hybrid density
871 functionals, J. Chem. Phys. 128 (8) (2008) 084106. arXiv:<http://dx.doi.org/10.1063/1.2834918>,
872 doi:10.1063/1.2834918.
873 URL <http://dx.doi.org/10.1063/1.2834918>
- 874 [100] J.-D. Chai, M. Head-Gordon, Long-range corrected hybrid density functionals with
875 damped atom–atom dispersion corrections, Phys. Chem. Chem. Phys. 10 (2008) 6615–6620.

876 doi:10.1039/B810189B.
877 URL <http://dx.doi.org/10.1039/B810189B>

878 [101] H. Iikura, T. Tsuneda, T. Yanai, K. Hirao, A long-range correction scheme for generalized-
879 gradient-approximation exchange functionals, *J. Chem. Phys.* 115 (8) (2001) 3540–3544.
880 arXiv:<http://dx.doi.org/10.1063/1.1383587>, doi:10.1063/1.1383587.
881 URL <http://dx.doi.org/10.1063/1.1383587>

882 [102] Y. Zhao, D. G. Truhlar, Density functional for spectroscopy: No long-range self-interaction
883 error, good performance for rydberg and charge-transfer states, and better performance on
884 average than b3lyp for ground states, *J. Phys. Chem. A* 110 (49) (2006) 13126–13130.
885 arXiv:<http://dx.doi.org/10.1021/jp066479k>, doi:10.1021/jp066479k.
886 URL <http://dx.doi.org/10.1021/jp066479k>

887 [103] Y. Zhao, D. G. Truhlar, Comparative dft study of van der waals complexes: Rare-gas dimers,
888 alkaline-earth dimers, zinc dimer, and zinc-rare-gas dimers, *J. Phys. Chem. A* 110 (15) (2006)
889 5121–5129. arXiv:<http://dx.doi.org/10.1021/jp060231d>, doi:10.1021/jp060231d.
890 URL <http://dx.doi.org/10.1021/jp060231d>

891 [104] T. Le Bahers, C. Adamo, I. Ciofini, A qualitative index of spatial extent in charge-transfer exci-
892 tations, *J. Chem. Theory Comput.* 7 (8) (2011) 2498–2506.

893 [105] D. Jacquemin, T. Le Bahers, C. Adamo, I. Ciofini, What is the "best" atomic charge model to
894 describe through-space charge-transfer excitations?, *Phys. Chem. Chem. Phys.* 14 (2012) 5383–
895 5388.

896 [106] T. H. Dunning, Gaussian basis sets for use in correlated molecular calculations. i. the atoms boron
897 through neon and hydrogen, *J. Chem. Phys.* 90 (1989) 1007–1023.

898 [107] R. A. Kendall, T. H. Dunning, R. J. Harrison, Electron affinities of the first-row atoms revisited.
899 systematic basis sets and wave functions, *J. Chem. Phys.* 96 (1992) 6796–6806.

900 [108] D. E. Woon, T. H. Dunning, Gaussian basis sets for use in correlated molecular calculations. iv.
901 calculation of static electrical response properties, *J. Chem. Phys.* 100 (1994) 2975–2988.

902 [109] J. R. Lakowicz, *Principles of Fluorescence Spectroscopy*, 3rd edition, Springer, 2006.

903 [110] G. V. Bünau, J. b. birks: *Photophysics of aromatic molecules*. wiley-interscience, london 1970.
904 704 seiten. preis: 210s, *Berichte der Bunsengesellschaft für physikalische Chemie* 74 (12) (1970)
905 1294–1295.

906 [111] A. G. Al-Sehemi, M. Pannipara, A. Kalam, A. M. Asiri, A combined experimental and compu-
907 tational investigation on spectroscopic and photophysical properties of a coumarinyl chalcone, *J.*
908 *Fluoresc.* 26 (4) (2016) 1357–1365.

909 [112] G. Garcia, C. Adamo, I. Ciofini, Evaluating push-pull dye efficiency using td-dft and charge transfer
910 indices, *Phys. Chem. Chem. Phys.* 15 (2013) 20210–20219.

- 911 [113] S. S. Bag, M. K. Pradhan, R. Kundu, S. Jana, Highly solvatochromic fluorescent naphthalim-
912 ides: Design, synthesis, photophysical properties and fluorescence switch-on sensing of ct-dna,
913 *Bioorganic Med. Chem. Lett.* 23 (1) (2013) 96–101.
- 914 [114] O. A. Kucherak, L. Richert, Y. Mély, A. S. Klymchenko, Dipolar 3-methoxychromones as bright
915 and highly solvatochromic fluorescent dyes, *Phys. Chem. Chem. Phys.* 14 (2012) 2292–2300.
- 916 [115] W. A. Wassam, E. C. Lim, "proximity effect" in radiationless transitions, *J. Chem. Phys.* 68 (2)
917 (1978) 433–454.
- 918 [116] S. Fery-Forgues, M. T. Le Bris, J. C. Mialocq, J. Pouget, W. Rettig, B. Valeur, Photophysical
919 properties of styryl derivatives of aminobenzoxazinones, *J. Phys. Chem.* 96 (2) (1992) 701–710.
- 920 [117] V. Gulbinas, G. Kodis, S. Jursenas, L. Valkunas, A. Gruodis, J.-C. Mialocq, S. Pommeret,
921 T. Gustavsson, Charge transfer induced excited state twisting of n,n-dimethylaminobenzylidene-
922 1,3-indandione in solution, *J. Phys. Chem. A* 103 (20) (1999) 3969–3980.
- 923 [118] K. Rurack, M. L. Dekhtyar, J. L. Bricks, U. Resch-Genger, W. Rettig, Quantum yield switching
924 of fluorescence by selectively bridging single and double bonds in chalcones: Involvement of two
925 different types of conical intersections, *J. Phys. Chem. A* 103 (48) (1999) 9626–9635.
- 926 [119] A. M. Asiri, S. A. El-Daly, S. A. Khan, Spectral characteristics of 4-(p-n,n-dimethyl-
927 aminophenylmethylene)-2-phenyl-5-oxazolone (dpo) in different media, *Spectrochim. Acta A* 95
928 (2012) 679 – 684.
- 929 [120] B. Jędrzejewska, P. Krawczyk, M. Józefowicz, Experimental and theoretical studies of the influ-
930 ence of solvent polarity on the spectral properties of two push-pull oxazol-5-(4h)-one compounds,
931 *Spectrochim. Acta A* 171 (2017) 258 – 267.
- 932 [121] D. Jacquemin, V. Wathelet, E. Perpète, C. Adamo, Extensive td-dft benchmark: Singlet-excited
933 states of organic molecules, *J. Chem. Theory Comput.* 5 (2009) 2420–2435.
- 934 [122] A. Laurent, D. Jacquemin, Td-dft benchmarks: A review, *Int. J. Quant. Chem.* 113 (2013) 2019–
935 2039.
- 936 [123] D. Jacquemin, Excited-state dipole and quadrupole moments: Td-dft versus cc2, *J. Chem. Theory*
937 *Comput.* 12 (8) (2016) 3993–4003.
- 938 [124] C. Guido, B. Mennucci, G. Scalmani, D. Jacquemin, Excited state dipole moments in solution:
939 Comparison between state-specific and linear-response td-dft values, *J. Chem. Theory. Comput.*
940 14 (3) (2018) 1544–1553.
- 941 [125] D. Nardi, A. Tajana, R. Pennini, Heterocyclic compounds from 3,3-dimercapto-1-aryl-2-propen-1-
942 ones. note 2. condensation with o-aminophenol and o-aminophenol, *J. Heterocycl. Chem.* 12 (1)
943 (1975) 139–142.
- 944 [126] H. Stachel, Die darstellung einiger heterocyclen aus acylketen-derivaten (benzoxazole, benzothia-
945 zole, benzothiodiazine, chinazolone). über keten-derivate, x, *Arch. Pharm.* 296 (5) (1963) 337–343.

- 946 [127] (Du Pont de Nemours and Co., 1939, U.S. Patent 2323504, Preparation of omega-acyl-azoles).
- 947 [128] F. Stepanov, S. Davydova, Heterocyclic derivatives of methylketones, *Zh. Obshch. Khim.* 28 (1958)
- 948 891–896.
- 949 [129] F. Babichev, Y. Volovenko, Acylation of 2-methylbenzazoles with use of esters of carboxylic
- 950 acids, *Sov. Prog. Chem.* 43 (1977) 49–50.
- 951 [130] E. Rauch, P. Dickinson, J. Welsh, Preparation of 2-benzoylmethylbezoxazoles (1968, U.S. Patent
- 952 3375258).
- 953 [131] E. H. Sund, B. E. Donohue, T. K. Thomas, Synthesis of 2-(2-benzoxazolyl)-1-phenylethanone and
- 954 related ethanones, *J. Chem. Eng. Data* 24 (3) (1979) 253–253.
- 955 [132] R. A. M. O’Ferrall, B. A. Murray, ¹H and ¹³C nmr spectra of α -heterocyclic ketones and assignment
- 956 of keto, enol and enamionone tautomeric structures, *J. Chem. Soc. Perkin Trans. 2* (1994) 2461–
- 957 2470.
- 958 [133] I. Dzvinchuk, M. Lozinskii, A. Vypirailenko, C-mono- and dibenzoylation of 2-methylbenzimidazole
- 959 with use of benzoyl chloride, *Zh. Org. Khim.* 30 (1994) 909–914.
- 960 [134] G. Ciurdaru, M. Ciuciu, The acylation of 2-methylbenzazoles, *J. Prakt. Chem.* 321 (2) (1979)
- 961 320–322.
- 962 [135] H. De Silva, S. Chatterjee, W. Henry, C. Pittman, Synthesis of functionalized fused-ring heterocyc-
- 963 les from tautomers of 2-(thiazole, oxazole, benzothiazole, and benzoxazole)-1-phenylethenols and
- 964 1,3-diacyl chlorides or n-(chlorocarbonyl) isocyanate, *Synthesis* 44 (2012) 3453–3464.
- 965 [136] H. De Silva, W. Henry, C. Pittman, Reactions of keto-enol tautomers of 2-thiazolyl-, 2-oxazolyl-,
- 966 2-benzoxazolyl-, or 2-benzothiazolyl-1-phenylethenols with α,β -alkynyl esters: Syntheses of highly
- 967 functionalized fused-ring heterocycles, *Synthesis* 44 (2012) 3337–3352.
- 968 [137] E. R. T. Robinson, D. M. Walden, C. Fallan, M. D. Greenhalgh, P. H.-Y. Cheong, A. D. Smith,
- 969 Non-bonding 1,5-s \cdots o interactions govern chemo- and enantioselectivity in isothioureia-catalyzed
- 970 annulations of benzazoles, *Chem. Sci.* 7 (2016) 6919–6927.
- 971 [138] Z.-T. Huang, M.-X. Wang, A new route to 3h-1,5-benzodiazepines and heterocyclic ketene amins
- 972 from benzoyl substituted ketene dithioacetals and diamines, *Synthesis* 12 (1992) 1273–1276.
- 973 [139] Z.-T. Huang, M.-X. Wang, The synthesis and tautomerization of ketene amins with benzimida-
- 974 zoline ring, *Tetrahedron* 48 (1992) 2325–2332.
- 975 [140] J. Davoll, 58. the reaction of o-phenylenediamine with $\alpha\beta$ -unsaturated acids and with β -keto-esters,
- 976 *J. Chem. Soc.* (1960) 308–314.
- 977 [141] I. Dzvinchuk, A. M. Nesterenko, V. V. Polovinko, A. B. Ryabitskii, M. Lozinskii, Synthesis and
- 978 tautomerism of 2-phenacyl-1h-benzimidazoles and their hydrogen bromide salts, *Chem. Heterocycl.*
- 979 *Compd.* 47 (2011) 953–963.
- 980 [142] Y. Kubota, S. Tanaka, K. Funabiki, M. Matsui, Synthesis and fluorescence properties of thiazole-

- boron complexes bearing a β -ketoiminate ligand, *Org. Lett.* 14 (2012) 4682–4685.
- [143] Q. Liu, X. Wang, H. Yan, Y. Wu, Z. Li, S. Gong, P. Liu, Z. Liu, Benzothiazole-enamide-based bf_2 complexes: luminophores exhibiting aggregation-induced emission, tunable emission and highly efficient solid-state emission, *J. Mater. Chem. C* 3 (2015) 2953–2959.
- [144] L. F. Minuti, M. G. Memeo, S. Crespi, P. Quadrelli, Fluorescent probes from stable aromatic nitrile oxides, *Eur. J. Org. Chem.* (4) (2015) 821–829.
- [145] A. Matviitsuk, J. E. Taylor, D. B. Cordes, A. M. Z. Slawin, A. D. Smith, Enantioselective stereo-divergent nucleophile-dependent isothioureia-catalysed domino reactions, *Chem. Eur. J.* 22 (2016) 17748–17757.
- [146] M. V. Costa, A. Brembilla, D. Roizard, P. Lochon, Action of (2-benzothiazolyl) methyllithium with organic polar functions, *J. Heterocycl. Chem.* 28 (1991) 1541–1544.
- [147] Z. Zhang, T. Daynard, S. Wang, X. Du, G. Chopiuk, J. Yan, J. Chen, S. Sviridov, Pyrazolylbenzothiazole derivatives and their use as therapeutic agents (2004, Patent WO2004/11460).